

Behaviour of composite beams made using high strength steel

R. Shamass and K.A. Cashell

Brunel University London

Abstract

High strength steel (HSS), defined as material with a yield strength of between 460 and 700 N/mm², is becoming increasingly popular in appropriate construction projects owing mainly to its excellent strength to weight ratio. The current paper is concerned with the use of high strength steels in steel-concrete composite beams, which is a relatively new application. In order to investigate the behaviour of these members, a finite element numerical model is developed and validated using available test data. The model represents composite beams made from HSS acting together with either solid or profiled concrete slabs. It accounts for the geometrical and material nonlinearity as well as the nonlinearity caused by the shear connectors. An extensive parametric study is conducted in order to assess the influence of the most salient parameters such as material properties, shear connection, distribution of shear connectors and beam geometry on the response, in terms of the bending capacity, stiffness, slip distribution and failure mode. The numerical results are compared with current design provisions and new reduction factors are proposed in order to obtain safe and economical design solutions.

1 Introduction

This paper is concerned with the behaviour of composite beams made from high strength steel. Composite beams comprising concrete slabs connected to steel sections using shear connectors are increasingly common in modern structures such as bridges and high rise buildings. The composite performance of the steel and concrete provides excellent strength and stiffness whilst using both materials in an efficient manner. The amount of composite action that is achieved depends on the degree of shear connection which develops between the steel and concrete, and this affects the strength and stiffness of the composite beam. A well-designed composite member can lead to significant savings in terms of section depth, material consumption and overall cost, as well as lower environmental pollution and carbon footprint or reduced energy consumption [1].

The most efficient use of the materials' strengths is when the composite beam is subjected to positive bending. In this case, the steel beam is subjected to tensile stresses and the concrete slab is primarily subjected to compressive stresses, thus utilising the favourable attributes of each material in an efficient manner. A rigid-plastic analysis of a composite beam section indicates that the positive moment capacity of a member can be increased by as much as 120% relative to the bare steel beam through composite action [2]. Moreover, the concrete slab provides lateral-torsional buckling resistance to the top flange. The design of composite beams is covered in EN 1994-1-1 [3] which includes rules for members made using steel sections with a yield strength of up to 460 N/mm².

The current paper is concerned with composite beams made from high strength steel (HSS), defined herein as material with a minimum yield strength of 460 N/mm². Although high strength steel grades have been available for many years, they have recently seen an increase

in use owing to their favourable strength to weight ratio as well as the ever-increasing demand for structures to be more cost and environmentally efficient. The higher steel strength relative to normal steel can result in relatively smaller section sizes which creates savings due to an overall reduction in the steel weight. Moreover, lighter structures lead to smaller foundations as well as lower construction and transportation costs. Using HSS in long-span bridges can reduce the number of bridge supports required thus requiring a shorter construction programme. For these reasons, HSS can be a very attractive material in appropriate design applications.

In recent years, HSS has been the subject of intensive research from the structural engineering community in order to provide useful and efficient design data. The structural performance, failure modes and ductility of steel members made from HSS can be significantly different to those made from conventional mild steel. The vast majority of research into HSS has been focussed on bare steel sections. Researchers have investigated the behaviour of HSS columns (e.g. [4-8]), beams (e.g. [9-12]) as well as connections (e.g. [13-15]).

In contrast, there has been little attention given to the behaviour of composite beams made from HSS and concrete. As stated before, Eurocode 4 for composite design provides design rules for composite beams made from steel with a yield strength of up to 460 N/mm². For steel grades with a yield strength of less than 420 N/mm², the code adopts a rigid-plastic analysis approach for calculating the bending resistance of the composite beam which provides efficient results. For composite beams made from structural steel with a yield strength between 420 and 460 N/mm², and when the distance between the extreme fibre of the concrete slab in compression and the plastic neutral axis (x_{pl}) is between 15% to 40% of the overall member depth (h_{comp}), the design bending resistance is obtained by multiplying the bending moment resistance calculated from rigid-plastic analysis with a reduction factor (β). The reduction factor is linearly related to the ratio x_{pl}/h_{comp} .

As stated previously, there has been limited research into the behaviour of composite beams made using HSS, particular by researchers in Australia. Uy and Sloane [16] tested two composite beams under 4-point bending which were constructed using steel with a yield strength of 690 N/mm². More recently, Ban and Bradford [17] developed a finite element (FE) model to investigate the behaviour of simply-supported composite beams. The validated numerical model was used to study the effect of various structural steel grades (namely S235, S460, S690 and S960) and shear connection ratios (from 0.2 to 1.2) on the flexural behaviour of composite beams. The numerical results obtained from the parametric study were compared with the predictions from a rigid-plastic analysis. It was concluded that while the rigid-plastic model adopted in Eurocode 4 provides an accurate prediction for composite beams made from normal strength steel, it overestimates the bending strength of HSS composite beams. Therefore, steel reduction factors based on rigid-plastic analysis, similar to the 0.85 factor used for concrete strength in design, were proposed to obtain the bending capacity of composite beams with HSS. However, this numerical study was limited to just two different composite beams. Ban et al. [18] developed and validated a finite-element model of a simply-supported HSS composite beam subjected to sagging moments. An extensive parametric study was conducted to investigate the effect of material properties, cross-sectional dimensions, degree of shear connection, and initial imperfections on the rotational capacity of composite beams.

Following an analysis of the work done to date, it is clear that there is a need for more research into the behaviour of HSS composite beams in order to fully understand the effect that various parameters have on the performance and to enable the development of more efficient design rules. Moreover, there is no available data in the public domain about composite beams with profiled sheeting. In this context, the current paper proceeds with a description of a three-dimensional FE model which has been developed to further advance the understanding of composite beams made from HSS, with and without profiled sheeting. The model is validated using existing experimental results on composite beams [21, 26, 27, 28, 29 and 30] and numerical results [17] and then employed to study the influence of the most salient parameters such as the steel grade, concrete slab geometry, shear connection ratio, concrete properties and the x_{pl}/h_{comp} ratio. The effect of shear connector distribution on the bending capacity, initial stiffness and load-deflection response is also investigated for composite beams with either a full or partial shear connection. The numerical results are compared to those obtained from the rigid-plastic analysis approach used in Eurocode 4. Finally, based on the findings of this research, design guidance for composite beams made from HSS is proposed.

2 Development of the numerical model

2.1 General

The model has been developed using the ABAQUS finite element software [19], which is capable of achieving numerical convergence despite the geometric and material nonlinearities of the behaviour. In the following subsections, the key information relating to the model is discussed.

2.2 Material behaviour

2.2.1 Concrete

The concrete damaged plasticity (CDP) model in the ABAQUS library is employed for representing the material in the concrete slab. In this model, the material behaviour is defined in terms of the elastic, plastic, compressive and tensile properties. It assumes that the concrete will either fail in compression, through crushing, or tension, by cracking. In the current work, the Poissons ratio and density of concrete are taken as 0.2 and 2400 kg/m², respectively. In addition to the compressive and tensile constitutive relationships, a number of other parameters are required in the CDP model, including: (i) dilation angle; (ii) eccentricity; (iii) ratio of the strength in the biaxial state to the strength in the uniaxial state (f_{b0}/f_{c0}); (iv) parameter K; and (v) viscosity parameter. These are assigned values of (i) 36°, (ii) 0.1, (iii) 1.16, (iv) 0.667, and (v) 0, respectively, in the current analysis.

The concrete is represented using the models given in Eurocode 2 [20], as shown in Fig. 1. In accordance with this, the stress-strain relationship for concrete (i.e. the σ_c - ϵ_c relationship) in compression is given as:

$$\sigma_c = \left(\frac{k \alpha - \alpha^2}{1 + (k - 2)\alpha} \right) f_{cm}, \quad 0 \leq \epsilon_c \leq \epsilon_{cu1} \quad (1)$$

In this expression, ϵ_{cu1} is the nominal ultimate strain and f_{cm} is the ultimate compressive strength of concrete, given by:

$$f_{cm} = f_{ck} + 8 \quad (2)$$

where f_{ck} is the characteristic cylinder strength. The parameters k and α are given by equations 3 and 4, respectively, in which ε_{c1} is the strain at the peak stress and E_{cm} is the elastic modulus of concrete:

$$\alpha = \frac{\varepsilon_c}{\varepsilon_{c1}} \quad (3)$$

$$k = 1.05 E_{cm} \frac{\varepsilon_{c1}}{f_{cm}} \quad (4)$$

In Eq. 4, ε_{c1} (as a percentage) is determined as:

$$\varepsilon_{c1} = 0.7(f_{cm})^{0.31} \leq 2.8 \quad (5)$$

The nominal ultimate strain (ε_{cu1}), as a percentage is given by:

$$\varepsilon_{cu1} = 2.8 + 27[(98 - f_{cm})/100]^4 \text{ for } f_{ck} \geq 50 \text{ N/mm}^2, \text{ otherwise } 3.5 \quad (6)$$

Additionally, the compressive damaged parameter (d_c) needs to be defined at each inelastic strain level. It ranges from zero, for undamaged material, to unity, when the material can no longer sustain any load. The value for d_c is obtained only for the descending branch of the stress-strain curve of concrete in compression as follows:

$$d_c = \frac{f_{cm} - \sigma_c}{f_{cm}} \quad \text{when } \varepsilon_c \geq \varepsilon_{c1} \quad (7)$$

Tension stiffening refers to the phenomenon whereby concrete continues to carry some tensile load even after cracking has taken place, though the tensile strength gradually decreases with increasing tensile strain. In the analysis, this property effectively simulates the interaction between the steel reinforcement and the surrounding concrete (i.e. bond). In this study, it has been assumed that once the tensile strength of concrete has been reached, the tensile strength decreases linearly to reach zero stress at a strain of 0.01. This value has been used by other researchers [17] and allows the analysis to run without significant numerical problems without compromising the accuracy of the results.

The tensile strength of concrete according to Eurocode 2 [20], is taken from the following formula:

$$f_t = 0.3f_{ck}^{2/3} \quad \text{for } f_{ck} \leq 50 \text{ N/mm}^2 \quad (8)$$

$$f_t = 2.12 \ln(1 + 0.1f_{cm}) \quad \text{for } f_{ck} > 50 \text{ N/mm}^2$$

Similarly to the simulation of concrete in compression, in the model, the tensile damaged parameter d_t must be defined at each increment of cracking strain. The value of d_t is valid only in the descending branch of the stress-strain curve for concrete in tension, as follows:

$$d_t = \frac{f_t - \sigma_t}{f_t} \quad (9)$$

in which f_t is the tensile strength of concrete and σ_t is the tensile stress of concrete corresponding to the tensile strain ε_t .

2.2.2 Steel

The steel beam in the composite member is modelled using a multi-linear stress-strain relation, as shown in Fig. 2. This relation is defined using young modulus E , yield stress f_y , yield strain ε_y , strain at the onset of hardening ε_{st} , ultimate stress f_u and corresponding ultimate strain ε_u . The stress-strain curves considered in the FE model are converted into true stress-strain relationships in order to consider the effects of the reduction of the cross-section during the tensile test. The formulae for conversion in terms of stress (σ) and strain (ε) are given by:

$$\begin{aligned} \sigma^{\text{true}} &= \sigma(1 + \varepsilon) \\ \varepsilon^{\text{true}} &= \ln(1 + \varepsilon) \end{aligned} \quad (10)$$

2.3 Geometry and element types

For composite beams with solid slabs sections, the steel beam, concrete slab and stiffeners (where applicable) are modelled using shell elements with reduced integration, namely the S4R element in ABAQUS [20]. The reduced integration enables more efficient computation without compromising the accuracy of the results. This element is widely used for construction applications because it is suitable for both thin and thick shells. The soffit of the concrete slab and the upper surface of the top flange of the steel beam are selected as a reference surface (Fig. 3). The steel reinforcement in the concrete slab is modelled using the rebar layer available in ABAQUS which is defined using the cross-sectional area of the steel reinforcement, the spacing of the bars, the position of the centroid of the reinforcing bars within the slab depth and the direction of the bars in the concrete slab.

For composite beams with profiled slabs on steel sheeting, the concrete slabs are modelled using reduced integration solid elements, named C3D8R in ABAQUS, whilst the reinforcement is modelled using truss elements (namely T3D2 in the ABAQUS library) which are embedded in the slab elements. Solid elements are used in order to represent that variable thickness of the slab. The steel beam section in these members as well as the steel decking and stiffeners are modelled using reduced integration shell element (S4R).

2.4 Modelling of the shear connectors

The shear studs are modelled using the Cartesian connector element available in the ABAQUS library, as reported by other researchers [e.g. 21, 22]. These elements connect a node in the beam flange with a coincident node in the slab at the connector location. The nonlinear behaviour of the connector element is defined in both the shear and axial directions. Failure of the connector is governed by the relative displacement of the element exceeding a user-defined limiting slip capacity (Δ_u).

The load-slip relationship of the shear connectors is modelled using the relation presented by [23], given as:

$$Q = Q_u(1 - e^{-0.71\Delta})^{2/5} \quad (11)$$

where Q is the shear force on the shear stud, Q_u is the ultimate capacity of the shear stud and Δ is the slip in millimetres (see Fig. 4).

The analytical formula presented in Eq. 11 is based on the results from pushout tests which were conducted to obtain the load-slip curve for shear connectors embedded in a solid concrete slab. Therefore, it is important to check the validity of this formula for modelling shear connectors embedded in profiled slabs. Fig. 5 presents an experimental load-slip response for shear studs embedded in a profiled slab with trapezoidal sheeting from an experimental programme [24], together with the corresponding analytical relationship predicted using Eq. 11. It is evident that the two curves are in excellent agreement, thus justifying the use of the analytical formula for profiled as well as flat slabs.

2.5 *Boundary and loading conditions*

In general, load is applied in the model through concentrated point loads, operated in displacement-control, in locations along the member which are defined by the user. The position of contact is defined as being the boundary between the bottom of the slab and the top surface of the steel beam. A hard contact point without friction is employed in order to enable the concrete and steel to separate during loading. A tie contact is defined between the surface of steel section and the edges of the stiffeners. The element size used in the numerical model is 20mm in each direction. A mesh sensitivity analysis was performed and it was found that using either a coarser or more refined element size did not alter the results presented.

2.6 *Solution method*

The ABAQUS software offers a number of solution strategies for structural problems. Following a literature review, it was found that researchers have used various methods for nonlinear structures similar to those discussed herein, with the most popular being the modified Riks arc-length method [25] and the implicit dynamic solution method. However, a conclusive agreement on the best approach was not readily available. Therefore, both were investigated in the current study in order to identify the most appropriate solution procedure.

In the modified Riks method, both the nodal displacement increments and the displacement multiplier increment are assumed to be unknown at each step. On the other hand, the implicit dynamic solution uses an implicit time integration scheme to calculate the transient dynamic or quasi-static response of a system. It can be used for quasi-static applications by introducing an inertia effect which regularizes unstable behaviour in analyses where the main focus is a final static response [19].

It was found that modified Riks method is only able to achieve convergence for some of the specimens analysed. However, the implicit dynamic solution method provides good convergence behaviour for all specimens assessed in the current study and is therefore adopted for all discussions hereafter.

3 Validation of the finite element model

The FE model described in the previous section has been validated using available test data [21, 26, 27, 28, 29 and 30]. Of these test programmes, only two [28, 29] included composite specimens made from high strength steel; the other test specimens were made using mild steel beams. However, in order to conduct a robust validation exercise, the beams made from mild steel are also included herein. Full details on these test programmes are available in the above-listed publications and the names of the specimens used in the validation exercise are given in Table 1. It is noteworthy that stiffeners were employed in all tested beams, apart from those tested by Chapman and Balakrishnan [26], at the support and loading positions.

3.1 Load-displacement response

Fig. 6 presents the load versus mid-span deflection data from both the FE model and also the experiments. For brevity, only one curve from each of the six test programmes (namely D1, CB1, HASAA-30BS, SCB2, Beam 1 and SB3) are presented herein as these are reflective of the results for all specimens. Specimens D1, CB1, SCB2, Beam 1 and SB3 failed by crushing of the concrete slab, and while HASAA-30BS failed by failure of the shear connectors. It is observed that the initial bending stiffness obtained by the FE model is in good agreement with the corresponding experimental value. Moreover, the failure modes observed experimentally are well predicted by the FE model including crushing of the concrete slab (e.g. in Specimen CB1 and failure of the shear connectors (e.g. in specimen HASAA-30BS). It is noteworthy that the FE model does not capture the softening behaviour in the load-deflection response, which was evident in the experimental curve for test SCB1. This is owing to the fact that the stress-strain curve for concrete in compression suggested by Eurocode 2 is defined only up to the ultimate strain ϵ_{u1} (see Fig. 1). Nevertheless, the FE model captures the overall strength, stiffness and failure mode of the test specimen with reasonable accuracy.

3.2 Ultimate load of the composite beams

The numerical results predicted by the FE model for the ultimate load of the composite beams are presented together with the experimental values in Fig. 7. It can be seen that the predicted ultimate loads are in good agreement with the corresponding experimental results. The average deviation is about $\pm 1\%$. Consequently, it can be concluded that the FE model developed in this study is adequate for predicting the bending strength of composite beams for specimens made from various concrete and steel materials, as well as different levels of shear connection.

3.3 Load-end slip and load-strain response

The load versus end-slip data from a small number of tests was available and therefore used to validate this information from the FE model. The end-slip is defined as the relative displacement that occurred at the interface between the steel and the concrete. Fig. 8(a) and (b) present the load versus end-slip data for specimens D1 [26] and HTFGB-30BS [21], respectively. These tests are selected in order to demonstrate the response for beams with full interaction (i.e. D1) and also partial shear interaction (i.e. HTFGB-30BS). The graphs show good agreement between numerical and experimental end-slip results. However, referring to Fig. 8(a) for specimen D1, it is evident that there is some disparity in the results at relatively low levels of load as the numerical model predicts greater levels of slippage. This difference is most likely due to the fact that friction between the steel and the concrete is not considered in the numerical model. Once this friction is overcome, the numerical and experimental

values coalesce. This disparity at low levels of deflection was not observed in specimen HTFGB-30BS, as this used pre-cast concrete slabs rather than in-situ concrete used in D1. It is also noteworthy that the order of magnitude of the end-slip data between these two tests are quite different owing to the different levels of shear interaction which were present.

The strain values at the bottom flange of the steel beam were measured during the testing of Beam 5 in the tests by Sedlacek and Hegger [29]. These are presented in Fig. 9 together with the corresponding numerical data from the FE model. It is evident that the FE model is in good agreement with the experimental data.

In addition to comparing the results from the developed numerical model with available test data, as discussed already in this paper, the model was also validated against published data obtained from another FE model, developed by Ban and Bradford [17]. This publication is relevant because it is directly concerned with composite beams made from HSS. It considers a simply-supported composite beam with different steel grades (namely S235, S460, S690 and S960) and shear connection ratios (from 0.2 to 1.2); further details are available elsewhere [17]. The main difference between the numerical model developed by Ban and Bradford [17] and that proposed in the current study lies in the solution method. Ban and Bradford [17] used the modified Riks method while the current study uses dynamic implicit method with quasi-static which has resulted in better convergence behaviour than the Riks method. The load-deflection curves found from the current FE model were compared with those published for the degree of shear connection $\eta=1$ and the results are presented in Fig. 10. It is observed that there is excellent agreement between the numerical results calculated from the present numerical model and those reported by Ban and Bradford.

On the basis of data presented in this section, it can be concluded that the FE model developed in this study is capable of providing a good prediction of the behaviour of composite beams in terms of the bending moment capacity, interaction performance and initial bending stiffness for members with full or partial shear connection as well as those made from either normal or high strength steel. Therefore, in the following sections of this paper, the model is used to investigate the effect that the most salient parameters have on the behaviour and to assess current design provisions.

4 Parametric study

In this section the model is used to conduct a study into the most influential parameters on the behaviour of composite beams made from high strength steel. These include steel grade, degree of shear connection, distribution of shear connectors, concrete strength, slab width and slab type. A large number of numerical simulations have been conducted in order to assess how each of these parameters affects the performance. All members were assumed to be simply supported with a single concentrated point load at the mid-point of the beam.

The high strength steel grades included in the study are S460 and S690, whilst the concrete grades considered are C40, C50 and C60. The shear connection ratio (η) ranges between 0.5 and 1.70. In this study, η is determined as the ratio between the force transferred by the shear connectors (N_{studs}) and the compressive force in the concrete flange at full shear connection ($N_{c,f}$), as defined by the Steel Construction Institute [31]. N_{studs} is the product of the strength of a single shear connector (P_{stud}) and the number of shear connectors in the shear span n . On

the other hand, $N_{c,f}$ is taken as being the lesser of either the axial resistance of the concrete slab and the axial resistance of the steel beam. Therefore, in the FE model, the strength of shear connection is calculated using the following expression:

$$P_{stud} = \eta N_{c,f} / n \quad (12)$$

Two steel beam sections (with an overall height of either 300 or 544 mm) and various widths of concrete slab ranging between 1000 mm to 4000 mm are considered in the parametric study. The geometric details of the composite beams included in this parametric study are given in Table 2.

The stress-strain relationship for concrete in tension and compression are illustrated in Fig. 2 and the elastic modulus and tensile strength of concrete were determined according to Eurocode 2, as described previously. The steel is assumed to behave in an elastic, perfectly-plastic, response in the parametric study in order to compare the bending capacity obtained numerically with those obtained using the rigid-plastic analysis approach adopted in Eurocode 4 [3]. The elastic modulus of steel is taken as 212 GPa in the analysis and the yield stresses for HSS S460 and S690 is 460 N/mm² and 690 N/mm², respectively. The mechanical behaviour of the shear connectors is described using the method proposed by Ollgaard et al. [23], as shown Fig. 4. The ultimate shear capacity is determined using Eq. 12. The ultimate slip capacity of the shear stud (Δ_u) is assumed to have a value of 6 mm, in accordance with the guidance given in Eurocode 4.

The maximum bending moment results obtained from the numerical simulations (M_{FE}) are compared with the analytical plastic moment of resistance (M_{pl}). Fig. 11 presents the ratio of M_{FE} to M_{pl} for composite beams made from S460 steel with different levels of shear connection and also various concrete slab widths; Fig. 11(a) is for C40 concrete whilst Fig. 11(b) represents the results for C50 concrete. The results were taken for composite beams S1 and S2 found in Table 2. Corresponding plots for composite beams made from S690 steel are illustrated in Fig. 12(a) and (b). It is evident from these figures that the general behaviour follows a very similar trend for all of the parameters investigated. That is, at low levels of shear connection (i.e. $\eta \leq 0.5$), the capacity predicted by the FE model is higher than that determined using rigid plastic analysis. The ratio of M_{FE} to M_{pl} generally reduces with increasing η for all specimens to a minimum value at $\eta = 1.0$. From this point, as the shear connection ratio increases, the ratio of M_{FE} to M_{pl} also increases. In the following subsections, these results are analysed in more detail with a view to investigating the influence of various salient parameters on the performance of composite beams made from HSS from a rigid-plastic analysis, considering the different shear connection ratios, in order to identify a suitable reduction factor for the predicted bending capacity of composite beam with steel grade S460 and S690.

4.1 Degree of shear connection

With reference to Figs. 11 and 12, it is observed that for beams with a shear connection ratio $\eta \leq 0.5$, rigid-plastic analysis generally provides conservative results for all slab widths examined in this study. From a shear connection ratio of 0.7 and above, the analytical moment of resistance tends to be higher than the numerical value, indicating an unconservative prediction. The maximum discrepancy between M_{FE} and M_{pl} typically occurs when $\eta = 1$. By

increasing the degree of shear connection beyond unity, the difference between the numerical and analytical results stabilises although the analytical values remain unconservative in almost all cases.

It is noteworthy that the flexural capacity of the composite beam, as predicted by the FE model, increases even when $\eta > 1.0$, despite the fact that theoretically, there is full shear connection once η equals unity. This indicates that for a composite beam with mechanical shear connectors, there must be some slippage at the interface between the concrete slab and steel beam in order to produce shear forces in the shear connectors. In reality, a full interaction, which is assumed in the rigid plastic analysis when η equals unity, cannot be achieved. In order to further investigate this phenomenon, Fig. 13 shows the stress distributions through the cross-section of a composite beam made from S460 steel, at the mid-span, obtained from both FE and rigid-plastic analysis. Two levels of shear connection are considered, namely η equal to a value of 1.0 or 1.7. It is observed that the stress distributions in the steel beam for the case where η equals 1.7 are closer to the assumed rectangular stress block than those obtained when η equals unity. For this reason, the bending resistance predicted by the FE model increases when η is greater than 1.0.

The effect that shear connection has on the load-deflection response is illustrated in Fig. 14(a) for composite beams with S460 steel and Fig. 14(b) for equivalent beams made from S690 steel. Section S2 as defined in Table 2 is employed in this analysis with C40 concrete and b_c equal to 1500 mm. It is clear that similar trends are observed, irrespective of the steel grade. The initial stiffness is greater for relatively higher levels of shear connection. As expected, the ultimate load generally increases with the level of shear connection up to a maximum value at η equal to unity. Beyond this, when $\eta > 1$, the ultimate load does not increase notably beyond the level when $\eta = 1$. The level of deflection at the ultimate load generally decreases with higher levels of shear connection, owing to the increased stiffness of the cross-section.

Clearly, the level of slip that occurs between the steel beam and the concrete slab is very influential to the overall behaviour, particularly in terms of ductility. Fig. 15 illustrates the slip that occurs along the length of the beam, at the interface between the steel and the concrete, for different values of η . The distance along the length of the beam has been normalised by the span of the beam being considered (i.e. L in Table 2). The results have been obtained for the S1 composite beam (Table 2) with a slab width of 1200 mm, C40 concrete and either S460 or S690 steel. The horizontal axis of the graph represents the distance from the mid-span along the length of the beam.

It can be seen that the slip at the interface is significantly greater for the composite beam made from S690 HSS compared with the S460 HSS. This is because the higher yield strength leads to greater load capacity and more relatively displacement between the two materials. As expected, greater levels of shear connection lead to less slippage at the interface. In addition, it is noteworthy that increasing the degree of shear connection from 0.5 to 1.0 leads to a more uniform distribution of slip over the length of the beam. Furthermore, the interface slip near the support (i.e. at a value of unity on the x-axis in Fig. 15(b)) for composite beam with a partial interaction is much higher than the slip along the rest of the beam length. This is discussed further in later sections of this paper where it is shown that in order to reduce the interface slip values near the support for beams with partial interaction, it is necessary to increase the concentration of shear connectors in this region.

4.2 *Material properties*

The effect that concrete strength has on the load-deflection response at the mid-span and slip that occurs along the length of the beam is illustrated in Fig. 16(a) and (b), respectively. The results were obtained for a S2 composite beam (see Table 2) with a slab width of 1200 mm, shear connection ratio of unity and S460 steel; the concrete strength was varied between C40, C50 and C60. It can be seen that the ultimate load increases slightly when the concrete slab is enhanced from C40 to C60, showing a slight contribution that the concrete strength makes towards the bending capacity of the composite beam. Also, the strength of concrete has no influence on the initial bending stiffness of the composite beam. However, the slip at the interface between the steel and the concrete at the failure load increases for relatively higher strength concrete. This is because the deflection at the ultimate load increases when a higher strength concrete is used, as shown in Fig. 16(a).

The effect that steel strength has on the load-deflection response at the mid-span and the slip that occurs along the length of the beam is illustrated in Fig. 17(a) and (b), respectively. The results were obtained again for a S1 composite beam with a slab width of 1200 mm, $\eta = 1$ concrete and C40 concrete. It can be seen that as expected, the ultimate load increases significantly when using a higher strength steel. In addition, the yield strength of steel has also no influence on the initial bending stiffness of the composite beam. However, Fig.17(b) illustrates that the level of slip at the interface at the failure load rises by increasing the yield strength of the steel. Similarly for higher strength concrete as previously discussed, this is because the deflection at failure is higher when a steel beam made from a relatively stronger material is employed in the composite section (Fig. 17(a)).

4.3 *Distribution of shear connectors*

In this section, the effect of the shear connectors' distribution on the flexural behaviour of composite beam is investigated, including the bending capacity, initial stiffness, load-deflection response and the shear forces that are induced in the shear studs. Two beams from the validation exercise previously described are chosen for the study, namely Beam 1 and HASSA-30BS (see Table 1). In the test programme, Beam 1 had a full shear connection and the failure mode was dominated by crushing of the concrete slab. On the other hand, HASSA-30BS had a partial shear connection and its failure mode was stud failure. The number of shear studs in the shear span for the specimens Beam 1 and HASSA-30BS were 36 and 16, respectively.

For Beam 1, four different distributions of shear connector are considered in the current analysis:

- (i) UN1: uniform distribution of shear connectors along the full length of the beam;
- (ii) N1: half of the shear connectors (i.e. 18) are concentrated in the support region of the beam, as shown in Fig. 18, with $x = L/3$ and the remaining shear connectors are distributed uniformly along the rest of the beam (i.e. $L - x$);
- (iii) N2: as case (ii) with $x = L/4$; and
- (iv) N3: as case (ii) with $x = L/6$.

For Beam HASSA-30BS, again four different shear connector distributions are considered in the analysis:

- (i) UN1: uniform distribution of shear connectors along the full length of the beam;

- (ii) NN1: half of the shear connectors (i.e. 8) are concentrated in the support region of the beam, as shown in Fig. 19(a), with $x_1 = L/4$, and the remaining shear connectors are distributed uniformly along the rest of the beam (i.e. $L - x$);
- (iii) NN2: as case (ii) with $x = L/6$; and
- (iv) NN3: 8 shear connectors are concentrated in the middle region of the beam (i.e. x_2 in Fig. 19(b)) whilst the remaining connectors are distributed uniformly along the rest of the beam (i.e. $L - x_2$, where $x_2 = L/4$).

Fig. 20(a) presents the load-deflection curves obtained from the four examples of shear connectors' distribution of the Beam 1. It can clearly be observed that distribution of the connectors' has little effect of the flexural response of the beam including the moment capacity and initial bending stiffness. However, with reference to Fig. 20(b) and (c), it is evident that having a greater concentration of shear connectors near the supports leads to significant variations in the end-slip experienced in the beam as well as the shear force in the connectors. The end-slip is reduced significantly when more shear connectors are placed near the supports, compared with a uniform distribution along the whole length. It is evident in Fig. 20(c) that having a uniform distribution of shear connectors along the length of the beam (i.e. UNI) leads to a uniform distribution of shear forces acting on the shear studs, except for the region near the mid-span (i.e. 0-0.2 on the x-axis in the figure). By having a greater concentration of connectors near the supports leads to a significant reduction in the level of shear force acting on the studs in this region (i.e. 0.8-1 on the x-axis in the figure) as well as a slight reduction in the shear forces on the connectors near the mid-span (0-0.2 on the x-axis in the figure). It is interesting to note that for the N1 distribution, there is a significant reduction in the shear forces acting on the connectors over the beam's length compared with uniformly distributed case.

Fig. 21(a) shows the load-deflection curves for the HASAA-30BS composite beam obtained from the different shear connector arrangements. As shown in the figure, the stud failure of the composite beam with concentrated shear connectors near supports (i.e. NN1 and NN2) occurs at a later point in the response, compared with the uniform connector distribution (UN1). This can be explained with reference to Fig. 21(b), where it is shown that the maximum slip at the interface between the steel beam and the concrete slab takes place near the supports and leads to failure of the shear connectors. By having a greater concentration of shear connectors in the region of the supports, the slip in this area and along the beam reduces significantly. On the other hand, concentrating the shear connectors near the mid-span, as in the case NN3, leads to early failure of the composite beam.

5 Design of composite beams made from HSS

Eurocode 4 [3] includes provisions for designing composite beams made from structural steel of nominal yield strength not more than 460 N/mm^2 . It allows rigid plastic theory to be used for Class 1 and 2 sections to determine the design moment of resistance (M_{pl}). For composite members made from HSS (i.e. S420 and S460), the code states that in order to avoid an overestimation of the bending capacity, where the distance between the plastic neutral axis and the extreme fibre of the concrete slab in compression (x_{pl}) exceeds 15% of the overall depth of the member (h_{comp}), the design resistance moment (M_{Rd}) should be multiplied by a reduction factor (β), determined as:

$$\beta = \begin{cases} 1 & \text{when } \frac{x_{pl}}{h_{comp}} \leq 0.15 \\ 1.09 - 0.6 \frac{x_{pl}}{h_{comp}} & \text{when } 0.15 < \frac{x_{pl}}{h_{comp}} \leq 0.4 \end{cases} \quad (13)$$

In this section, the validity of this design approach is investigated based on the findings presented herein.

In order to consider the design issues, it is necessary to understand the basis of design and how this is affected by using HSS. In this context, Fig. 22 presents the stress distribution at the mid-span obtained from the FE model as well as that assumed in rigid-plastic analysis (shown with dotted lines) for composite beams made from S460 and S690 steel. It is evident that there are significant differences between the stress-state predicted by the numerical and analytical models. The assumed rectangular stress-blocks in the rigid-plastic analysis lead to an overestimation of the bending strength of composite beams made from HSS. This is more prominent for the higher grade steel, S690 compared with beams made from S460 steel.

The flexural moment capacity of the beams defined previously in the parametric study (i.e. S1 to S4 in Table 2) have been analysed using the FE model and rigid-plastic analysis. For the purposes of this study, it is assumed that the shear connection ratio is unity. The HSS used in the study is either S460 or S690 and the concrete grades are C40, C50 or C60. The reduction factor calculated numerically using the ratio M_{FE}/M_{pl} is compared with those calculated using the rigid plastic analysis approach in Eurocode 4 and the results are presented in Fig. 23 for both composite beams made from both S460 and S690 structural steel.

It is evident from the figures that the β value obtained through numerical analysis for all concrete grades does not display the same trend as the Eurocode 4 formula. In the design code, the reduction factor reduces steadily as the ratio of plastic neutral axis depth (x_{pl}) to member depth (h_{comp}) increases. However, the current analysis shows that for beams made from S460 or S690 steel, there is no downward trend in M_{FE}/M_{pl} with increasing values of x_{pl}/h_{comp} . The behaviour is quite different from that defined in the design code and, moreover, it is evident that the existing Eurocode 4 reduction factors lead to potentially unconservative results with an overestimation of the ultimate bending capacity. As demonstrated by the dashed line in the figures, a lower bound reduction factor can be established whereby all the numerical results are on the conservative side. Based on the FE results, the reduction factor is suggested to be a constant value of $\beta_{prop} = 0.955$ for beams made from S460 and $\beta_{prop} = 0.94$ when S690 HSS is used. It is not appropriate to propose a reducing β with increasing x_{pl}/h_{comp} , for composite beams made from HSS with $\eta = 1$. These factors provide conservative predictions for the design bending moment resistance for composite beams made from HSS and with C40, C50 or C60 concrete. Although the results presented in this section are relevant only for the sections included in this study, the results demonstrate that the design codes in their current state are not suitable for composite beams made from HSS.

A similar study has been conducted for the same arrangement (i.e. composite beams with S460 or S690 steel and C40, C50 or C60 concrete) but with a shear connection equal to 1.7, in order to ensure a full shear connection in the finite element analysis; the results are presented in Fig. 24(a) and (b). In this instance, for the composite beams made from S460 steel, the ratio

of M_{FE}/M_{pl} does show some reduction with increasing values of x_{pl}/h_{comp} . However, for beams using S690 HSS, no reduction is evident. Therefore, it is concluded that the current Eurocode design provisions are inadequate for composite beams made from HSS with $\eta = 1.7$. The dashed lines in Fig. 24(a) and (b) illustrate new proposed reduction factors (β_{prop}), and these are represented by Eq. 14 for S460 and a constant value of $\beta_{prop} = 0.95$ for S690.

$$\beta_{prop} = \begin{cases} 1 & \text{when } \frac{x_{pl}}{h_{comp}} \leq 0.075 \\ 1.03 - 0.4 \frac{x_{pl}}{h_{comp}} & \text{when } 0.075 < \frac{x_{pl}}{h_{comp}} \leq 0.4 \end{cases} \quad (14)$$

6 Composite beams made from HSS and profiled concrete slabs

As composite construction becomes increasingly common, the use of profiled slabs acting compositely with steel beams is also seeing a rise in specification. In this context, in the current section, the effect of using HSS for these types of arrangements is investigated, as well as the effect that the degree of shear connection present has on the performance. The previously described numerical model is employed towards this end and the previously defined beam SB1 is used for illustrative purposes. It is assumed that the beam is simply supported and subjected to two point loading. The strength of shear connection is determined using Eq. 12 for which the number of shear connectors in the shear span is nine.

In this analysis, the shear connection ratio is varied between 0.2 and 1.40, the concrete compressive strength (f_{ck}) is taken as either 20, 40 or 60 N/mm² whilst the yield strength of the structural steel beam (f_y) is 235, 460 or 690 N/mm². Young's modulus of the structural steel beam is 212 GPa. The steel is assumed to behave in an elastic-plastic manner implying that any plastic hardening effects are ignored. This is in order to enable a direct comparison of the predicted bending capacity with equivalent values determined using rigid-plastic analysis as in Eurocode 4. As before, the mechanical behaviour of the shear connectors in the numerical analysis is described according to the method proposed by Ollgaard et al. [23]. The ultimate shear capacity is determined using Eq. 12 and the ultimate slip capacity of the shear stud Δ_u is assumed to be 6 mm.

The bending strength results obtained numerically (M_{FE}) are compared with the corresponding values determined using rigid-plastic analysis (M_{pl}), and the results are presented in Fig. 25. It is shown that the bending strength ratio decreases as the degree of shear connection rises. For composite beams with S460 HSS, the rigid-plastic analysis provides conservative predictions when $\eta \leq 0.5$. On the other hand, for higher levels of shear connection ratio, rigid-plastic analysis overestimates the bending strength and the overestimation reaches a peak when $\eta \leq 1.0$. For composite beams with S690 HSS, the rigid-plastic analysis overestimates the bending strength for all levels of shear connection studied herein.

In real structures, a partial shear connection often exists for composite beams with profiled sheeting due to the space limitation in the troughs for welding the shear connectors to the steel beam. Therefore, it is very important to relate the reduction factor (β) to η . By taking a line from the point corresponding to $\eta = 0.2$ to the point corresponding to $\eta = 1.0$ for each curve

(with reference to the dashed lines in Fig. 25), a relationship between the reduction factor and the degree of shear connection can be obtained, as follows:

$$\begin{aligned}\beta &= -0.117\eta + 1.057 \quad \text{for composite beams made from S460 HSS} \\ \beta &= -0.094\eta + 1.019 \quad \text{for composite beams made from S690 HSS}\end{aligned}\tag{15}$$

where β should be less than or equal to unity.

7 Conclusions

The use of high strength steel in civil engineering structures is becoming increasingly common in response to environmental demands. This paper has presented a study in the effect that using these materials in steel-concrete composite beams has on their behaviour as well as the consequences for designers. A finite element (FE) model was developed for composite beams and validated using existing experimental data, as reported in the literature. Following the verification of the model, it was employed to undertake an intensive parametric study in which several salient parameters were investigated. These include steel grade, degree of shear connection, distribution of shear connectors, concrete strength and slab geometry. Based on this work, the following conclusions are made:

- The FE data are in good agreement with experimental and numerical results, suggesting that the proposed model is accurate and reliable for predicting the performance of composite concrete-steel beams subjected to bending and constructed using either mild steel or HSS.
- For beams with a shear connection ratio $\eta \leq 0.5$, the rigid-plastic analysis method employed in Eurocode 4 provides slightly conservative results. However, for higher levels of shear connection, the discrepancy between the FE and Eurocode prediction increases, reaching a peak when $\eta = 1.0$. Therefore, based on FE results, new reduction factors for design are proposed for predicting the bending capacity of composite beams made from S460 and S690 HSS.
- The ultimate load generally increases with a rise in the degree of shear connection. Furthermore, the level of deflection at the ultimate load generally decreases with higher levels of shear connection.
- The slip at the interface between the steel section and concrete slab is significantly greater for composite beams made from S690 HSS compared with those using S460 HSS. Furthermore, the interface slip values near the supports for composite beams with partial interaction are significantly greater than those obtained over the rest of the beam. Therefore, it is recommended that designers specify a greater concentration of shear connectors in the region near the supports, thus preventing premature stud failure. Also, a greater concentration of shear connectors near the supports for beams with a full shear connection leads to a significant reduction in the level of shear forces acting in the studs in this region, as well as along the length of the beam in some cases.
- As expected, the bending capacity increases when stronger materials are used (especially higher strength steel). Moreover, the slip at the interface corresponding to the failure load increases when stronger materials are employed.
- New reduction factors have been proposed for different levels of shear connection, for composite beams with profiled steel sheeting and made from S460 and S690 HSS.

Acknowledgments

The support provided by Brunel University London through the BRIEF research fund for the work described in this paper is gratefully acknowledged.

References

- [1] Hauke, B. Economic application of composite beams with moderate high strength materials. In: Proceedings of the 5th European Conference on Steel and Composite Structures: 2008, Graz, Switzerland.
- [2] Kirkland, B., Kim, P., Uy, B., Vasdravellis, G. (2015). Moment–shear–axial force interaction in composite beams. *Journal of Constructional Steel Research*, 2015; 114:66-76.
- [3] EN 1994-1-1. Eurocode 4: Design of composite steel and concrete structures. Part 1-1 General rules and rules for buildings. CEN; 2004.
- [4] Rasmussen, K.J.R., Hancock, G.J. Tests of high strength steel columns. *Journal of Constructional Steel Research*, 1995; 34(1):27-52.
- [5] Ban, H., Shi, G., Shi, Y., Wang, Y. Overall buckling behavior of 460 N/mm² high strength steel columns: Experimental investigation and design method. *Journal of Constructional Steel Research*, 2012; 74:140-150.
- [6] Ban, H., Shi, G., Shi, Y., Bradford, M.A. Experimental investigation of the overall buckling behaviour of 960 N/mm² high strength steel columns. *Journal of Constructional Steel Research*, 2013; 88:256-266.
- [7] Wang, Y.B., Li, G.Q., Chen, S.W., Sun, F.F. Experimental and numerical study on the behavior of axially compressed high strength steel columns with H-section. *Engineering Structures*, 2012; 43:149-159.
- [8] Wang, Y.B., Li, G.Q., Chen, S.W., Sun, F.F. Experimental and numerical study on the behavior of axially compressed high strength steel box-columns. *Engineering Structures*, 2014; 58: 79-91.
- [9] Ricles, J.M., Sause, R., Green, P.S. High-strength steel: implications of material and geometric characteristics on inelastic flexural behaviour. *Engineering Structures*, 1998; 20(4):323-335.
- [10] Bradford, M.A., Lui, X. Flexural-torsional buckling of high-strength steel beams. *Journal of Constructional Steel Research*, 2016; 124:122-131.
- [11] Lee, C.H., Han, K.H., Uang, C.M., Kim, D.K., Park, C.H., Kim, J.H. Flexural strength, rotation capacity of I-shaped beams fabricated from 800-MPa steel. *Journal of Structural Engineering*, 2012; 139(6):1043-1058.
- [12] Ma, J.L., Chan, T.M., Young, B. Experimental investigation of cold-formed high strength steel tubular beams. *Engineering Structures*, 2016; 126:200-209.
- [13] Puthli, R., Fleischer, O. Investigations on bolted connections for high strength steel members. *Journal of Constructional Steel Research*, 2001; 57(3): 313-326.

- Shamass, R., Cashell, K.A. Behaviour of composite beams made using high strength steel. *Structures*, 2017. 12: 88-101. <http://www.sciencedirect.com/science/article/pii/S2352012417300528>
- [14] Coelho, A.M.G., Bijlaard, F.S. Experimental behaviour of high strength steel end-plate connections. *Journal of Constructional Steel Research*, 2007; 63(9):1228-1240.
- [15] Može, P., Beg, D., Lopatič, J. Net cross-section design resistance and local ductility of elements made of high strength steel. *Journal of Constructional Steel Research*, 2007; 63(11):1431-1441.
- [16] Uy, B., Sloane, R.J. Behaviour of composite tee beams constructed with high strength steel. *Journal of Constructional Steel Research*, 1998; 1(46):203-204.
- [17] Ban, H., Bradford, M.A. Flexural behaviour of composite beams with high strength steel. *Engineering Structures*, 2013; 56:1130-1141.
- [18] Ban, H., Bradford, M.A., Uy, B., Liu, X. (2016). Available rotation capacity of composite beams with high-strength materials under sagging moment. *Journal of Constructional Steel Research*, 2016; 118:156-168.
- [19] ABAQUS. ABAQUS User manual - Version 6.11. Hibbitt, Karlsson and Sorensen, Inc., USA. 2011.
- [20] EN 1992-1-1. Eurocode 2: Design of concrete structures. Part 1-1: general rules and rules for buildings. CEN; 2004.
- [21] Kwon, G., Engelhardt, M.D., Klingner, R.E. Experimental behavior of bridge beams retrofitted with postinstalled shear connectors. *Journal of Bridge Engineering*, 2011; 16(4):536-545.
- [22] Kmiecik, P., Kamiński, M. Modelling of reinforced concrete structures and composite structures with concrete strength degradation taken into consideration. *Archives of Civil and Mechanical Engineering*, 2011; 11(3):623-636.
- [23] Ollgaard, J.G., Slutter, R.G., Fisher, J.W. Shear strength of stud connectors in lightweight and normal weight concrete, *AISC Engineering Journal*, 1971; 8:55-64.
- [24] Smith, A.L., Couchman, G.H. Strength and ductility of headed stud shear connectors in profiled steel sheeting. *Journal of Constructional Steel Research*, 2010; 66(6):748-754.
- [25] Riks, E. An incremental approach to the solution of snapping and buckling problems. *International Journal of Solids and Structures*, 1979; 15(7):529-551.
- [26] Chapman J.C., Balakrishnan S. Experiments on composite beams. *Structure Engineering*, 1964; 42(11):369–83.
- [27] Vasdravellis, G., Uy, B., Tan, E.L., Kirkland, B. Behaviour and design of composite beams subjected to sagging bending and axial compression. *Journal of Constructional Steel Research*, 2015; 110:29-39.
- [28] Zhao, H., Yuan, Y. Experimental studies on composite beams with high-strength steel and concrete. *Steel and Composite Structures*, 2010; 10(5):373-383.
- [29] Sedlacek, G., Hegger, J. Use of high strength steel S460. ECSC Research Project Number 7210-SA/129, Final Report, 2002.
- [30] Nie, J., Fan, J., Cai, C.S. Experimental study of partially shear-connected composite beams with profiled sheeting. *Engineering Structures*, 2008; 30(1):1-12.
- [31] Steel Construction Institute. Composite design of steel framed buildings – in accordance with Eurocodes and the UK National Annexes. P359 Steel Construction Institute SCI; 2011.

Shamass, R., Cashell, K.A. Behaviour of composite beams made using high strength steel. Structures, 2017. 12: 88-101. <http://www.sciencedirect.com/science/article/pii/S2352012417300528>

Table 1: Test programmes used for validation of FE model.

Reference	Names of specimens used in validation	Loading and boundary conditions	Summary of test programme
Chapman and Balakrishnan [26]	A4, A5, B1, C1, D1, E1 and F1	Simply supported with concentrated point load applied at mid-span	Mild steel beams with solid concrete slabs and varying degrees of shear connections.
Vasdravellis et al. [27]	CB1	Simply supported with concentrated point load applied at mid-span	Mild steel beams with solid concrete slab
Kwon et al. [21]	DBLNB-30S, HTFGB-30BS and HASAA-30BS	Simply supported with concentrated point load applied at mid-span	Mild steel beams with solid concrete slabs and post-installed shear connectors
Zhao and Yuan [28]	SCB1, SCB2, SCB3	Simply supported with two concentrated point loads (4-point bending)	High strength steel beams with solid concrete slabs
Sedlacek and Hegger [29]	Beam 1, Beam 5, Beam 100 and Beam 300	Simply supported with concentrated point load applied at mid-span	High strength steel beams with solid normal- and high-strength concrete slabs
Nie et al. [30]	SB1, SB2 and SB3	Simply supported with two concentrated point loads (4-point bending)	Normal strength steel beams with profiled concrete slabs

Table 2: Details of the beams considered in the parametric study

Specimen	S1	S2	S3	S4
Span length, 2L (mm)	5500	1100	8000	14080
Slab width, b_c (mm)	1000 or 1200	1500, 2000, 2500 or 3000	1000, 1600 or 2000	2500, 3000, 3500 or 4000
Slab thickness, t_c (mm)	100	100	200	200
Total number of studs	80	160	100	176
Number of rows of studs	1	1	1	1
Stud spacing in longitudinal direction (mm)	68.75	68.75	80	80
Steel beam height, h (mm)	300	300	544.5	544.5
Width of the flange, b_f (mm)	150	150	211.9	211.9
Thickness of the flange, t_f (mm)	16	16	21.3	21.3
Thickness of the web, t_w (mm)	12	12	12.7	12.7

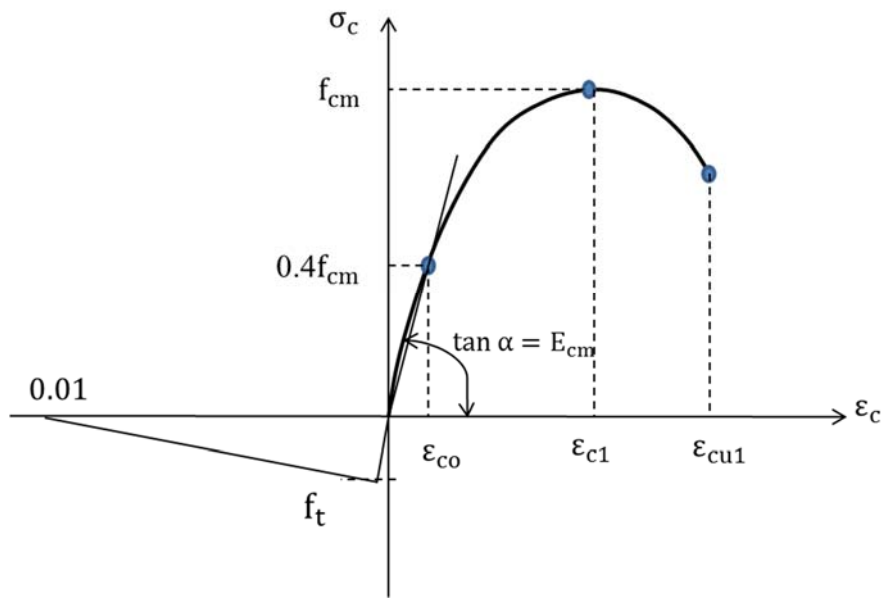


Figure 1: Stress-strain relationship for concrete in compression and tension used for structural analysis, as given in Eurocode 2 [20].

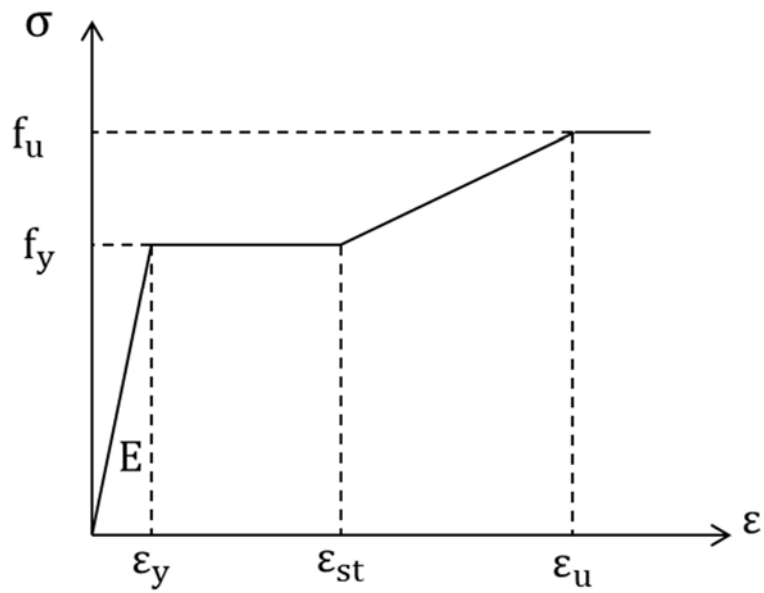


Figure 2: stress-strain relationship of steel material in steel beam

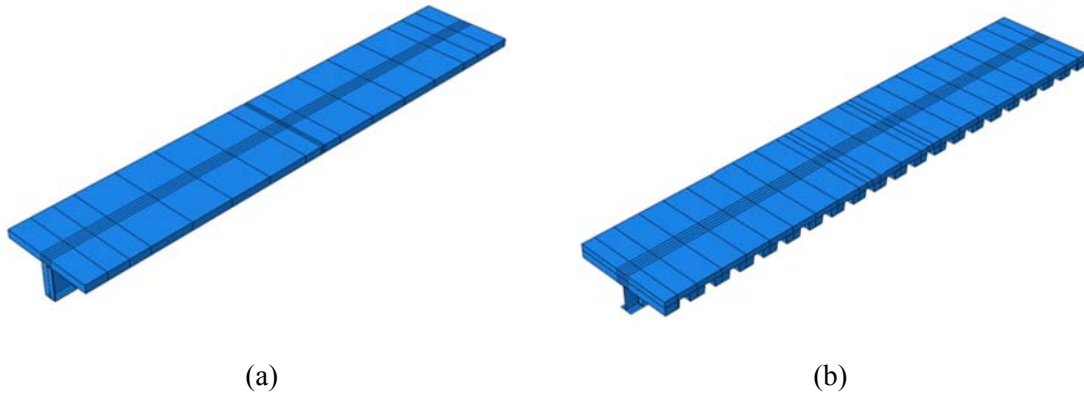


Figure 3: Finite element mesh of the composite beam with a (a) solid concrete slab and (b) profiled slab

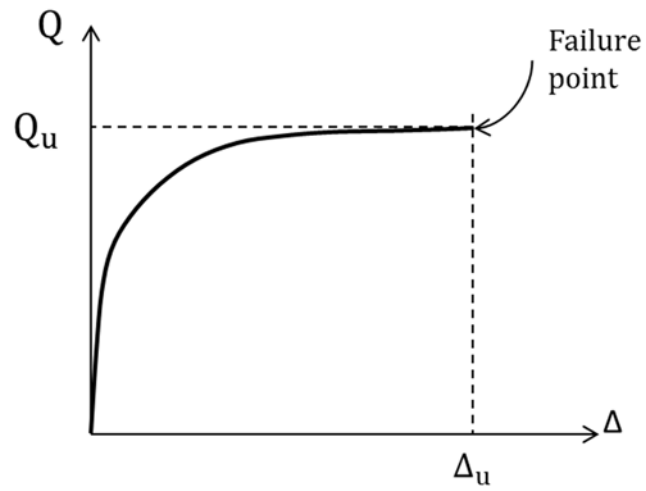


Figure 4: load-slip relationship of shear connectors

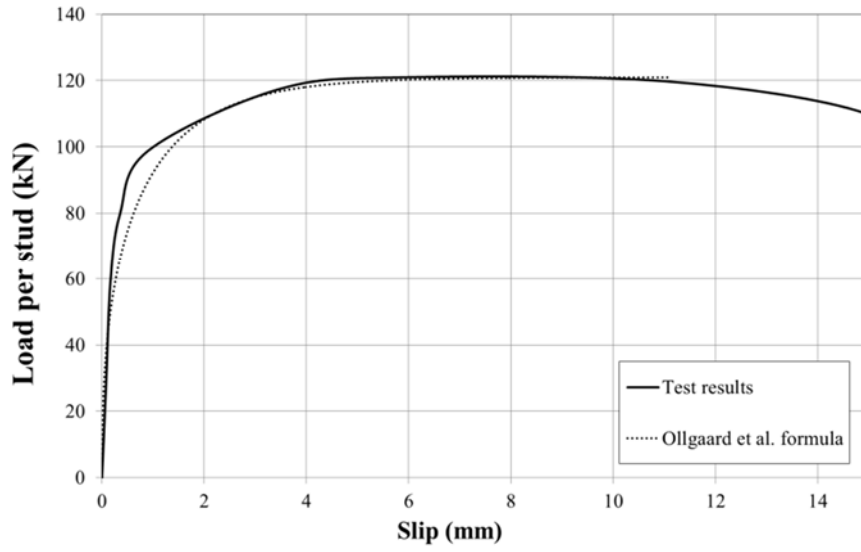
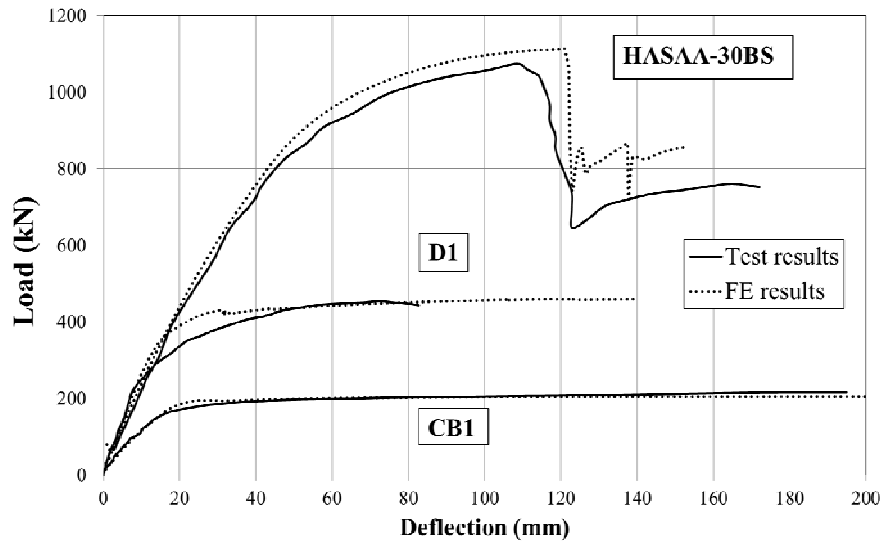
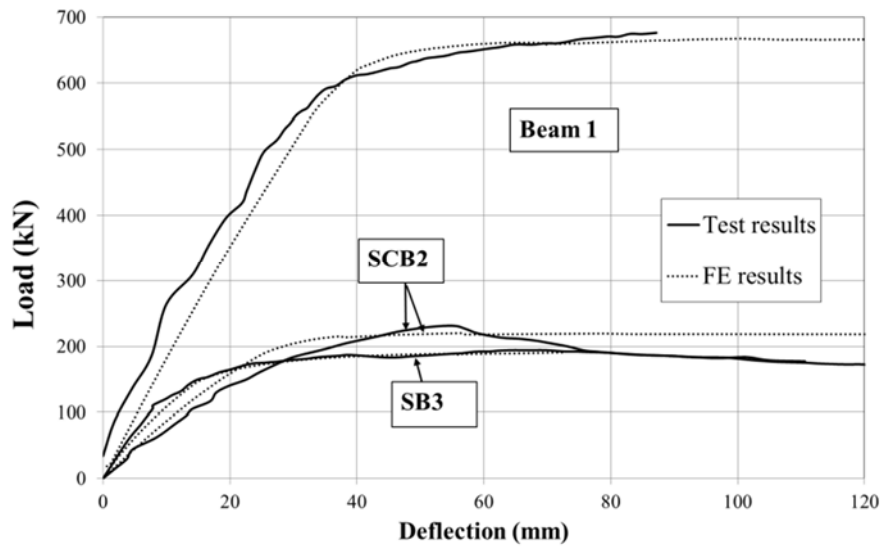


Fig. 5: Comparison between experimental results reported by [24] and analytical formula calculated using Ollgaard et al. [23] formula



(a)



(b)

Figure 6: Numerical and experimental load-displacement responses for (a) E1 [25], CB1 [26] and HASAA-30BS [21]; (b) SCB2 [28], Beam 1 [29], and SB3 [30].

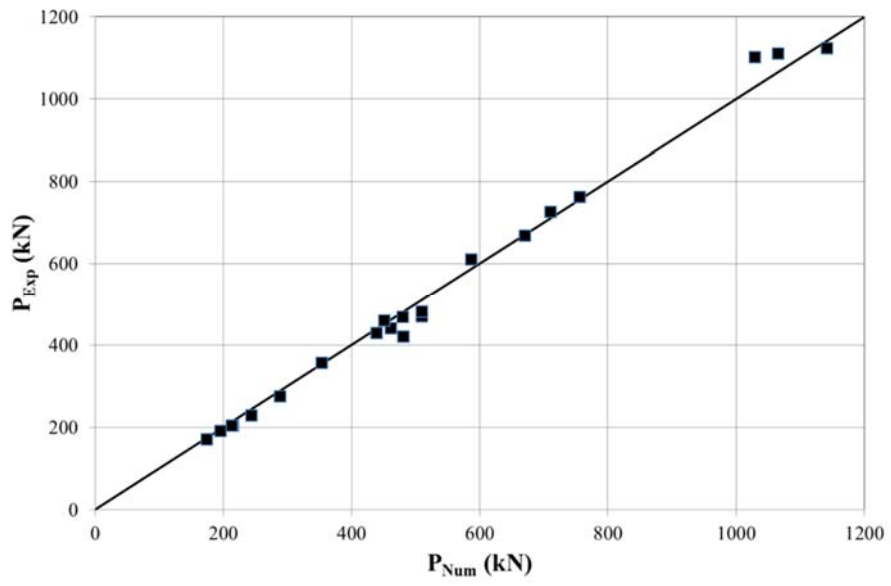
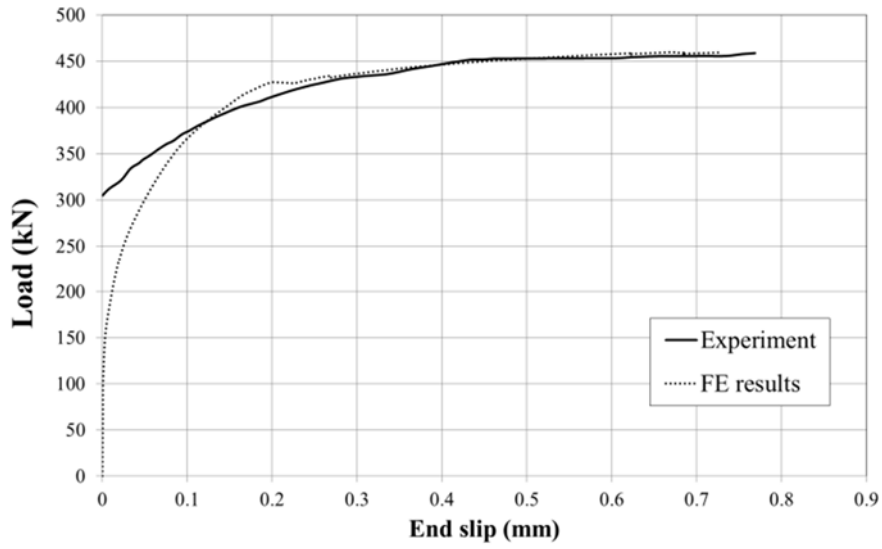
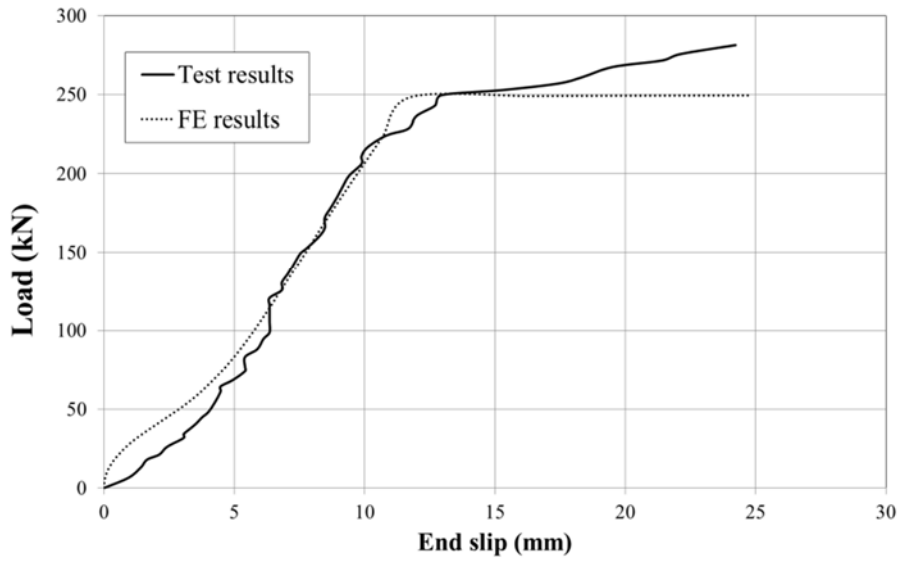


Figure 7: Comparison of the experimental and numerical ultimate load values



(a)



(b)

Figure 8: Load versus end-slip for specimens (a) D1 and (b) HTFGB-30BS

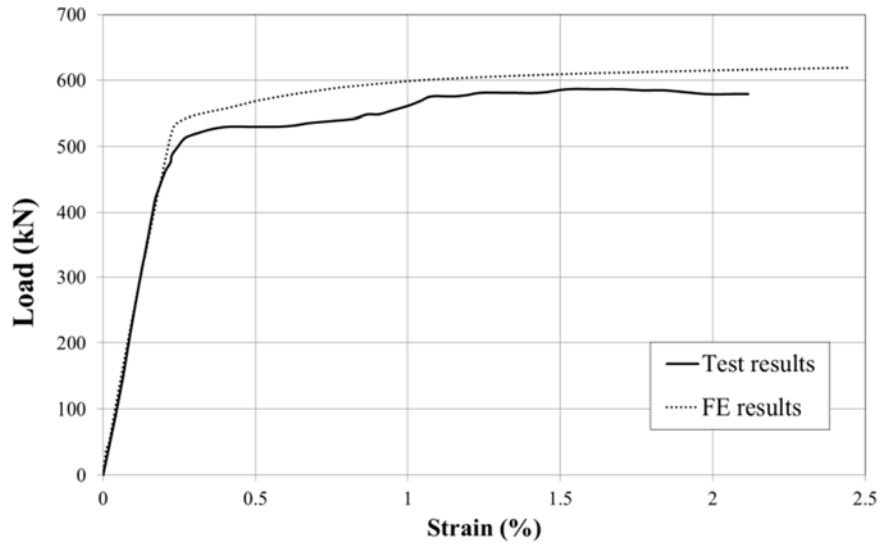


Figure 9: Experimental and numerical values for the load versus strain (measured on the bottom flange of the steel beam) for Beam 5 [29]

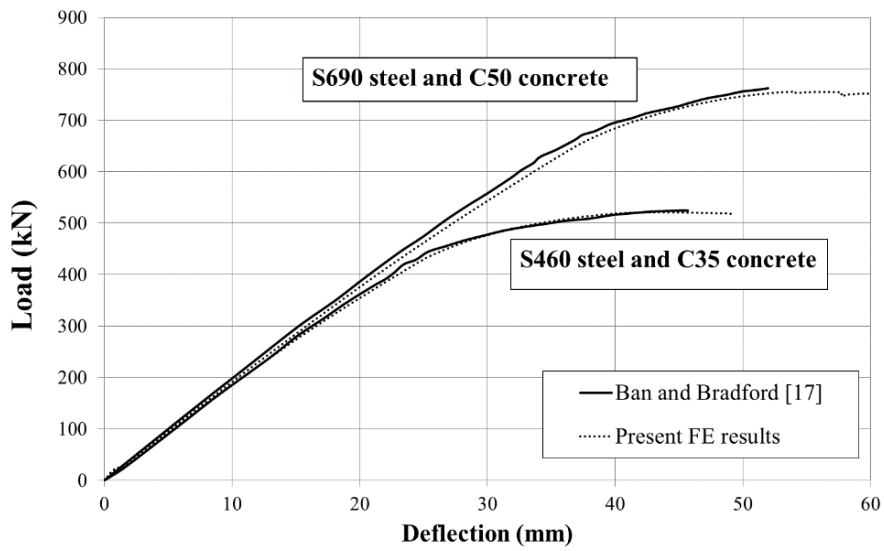
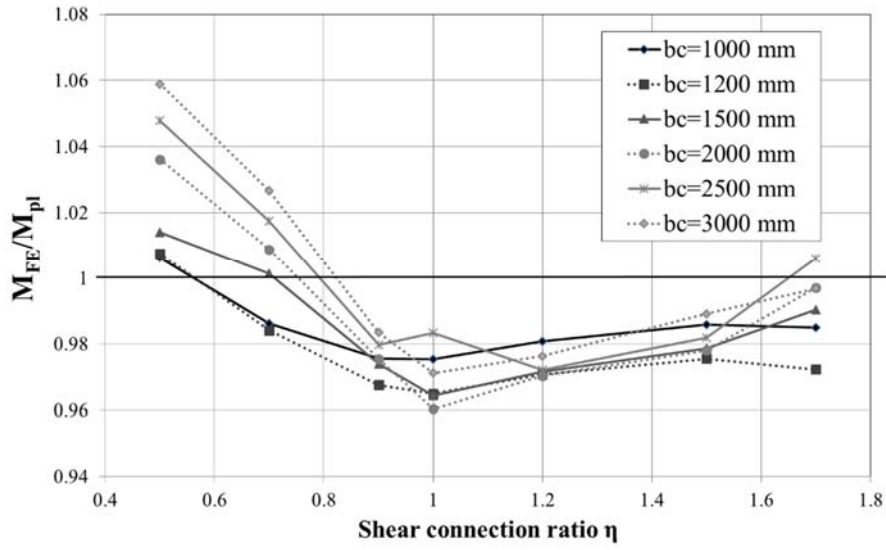
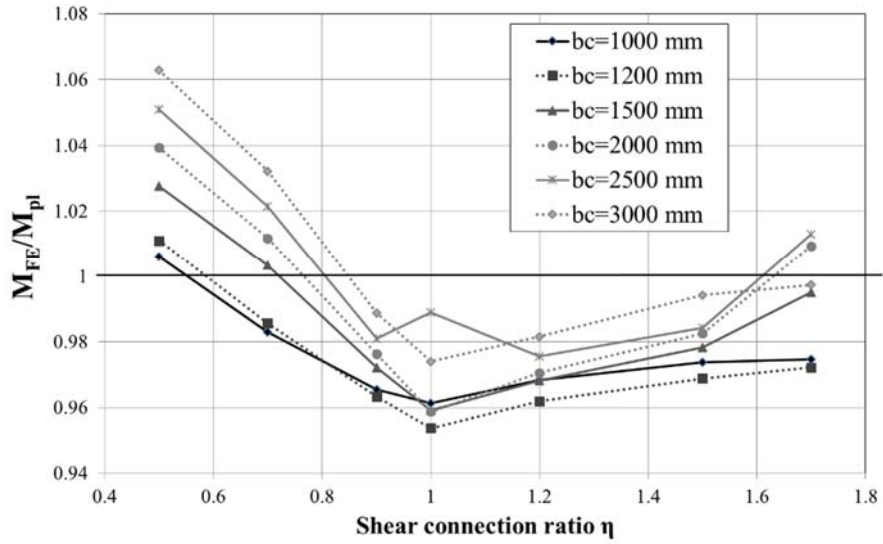


Figure 10: Comparison of load-deflection curves from the FE model developed in this study with those reported by Ban and Bradford [17]

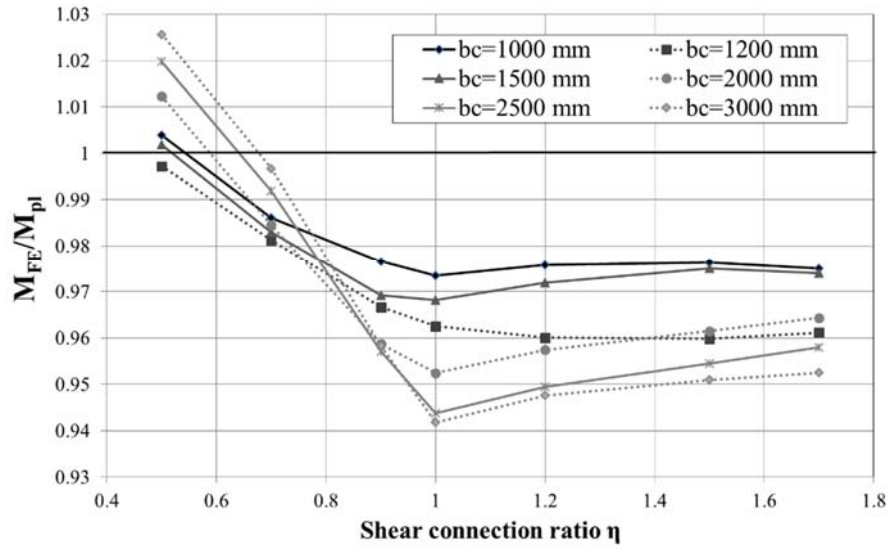


(a)

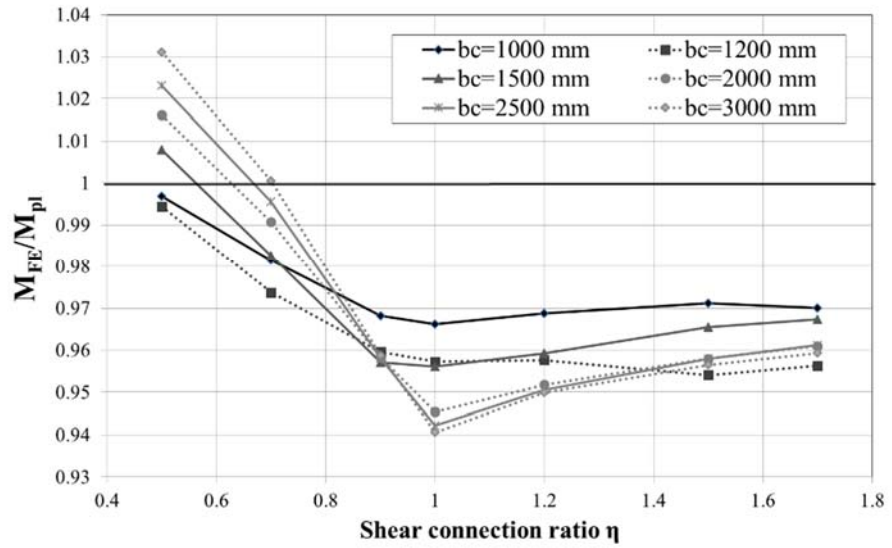


(b)

Figure 11: The effect of the degree of shear connection on the flexural capacity of a composite beam made from S460 HSS and (a) C40 concrete and (b) C50 concrete.



(a)



(b)

Figure 12: The effect of the degree of shear connection on the flexural capacity of a composite beam made from S690 HSS and (a) C40 concrete and (b) C50 concrete.

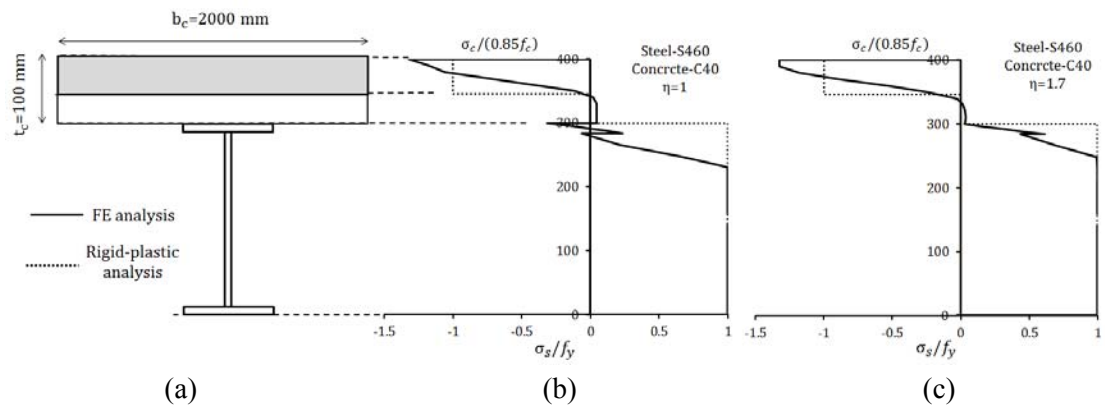
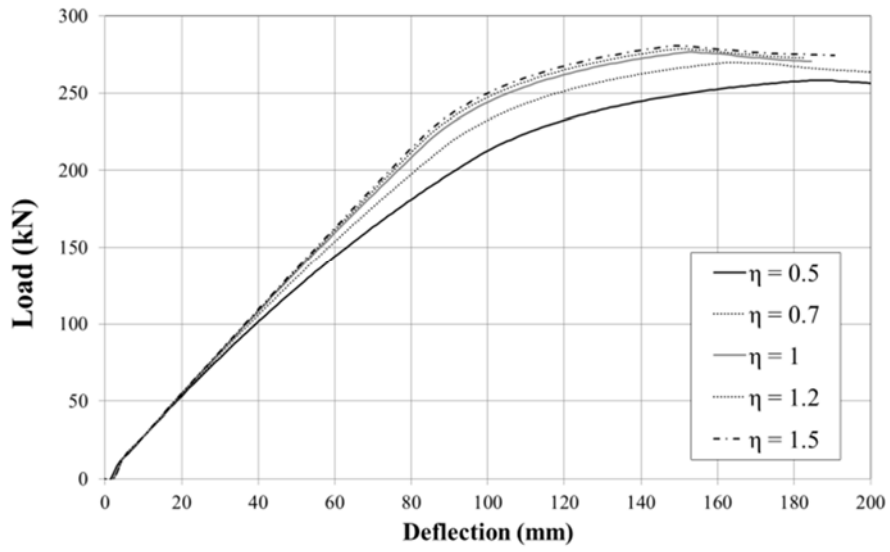
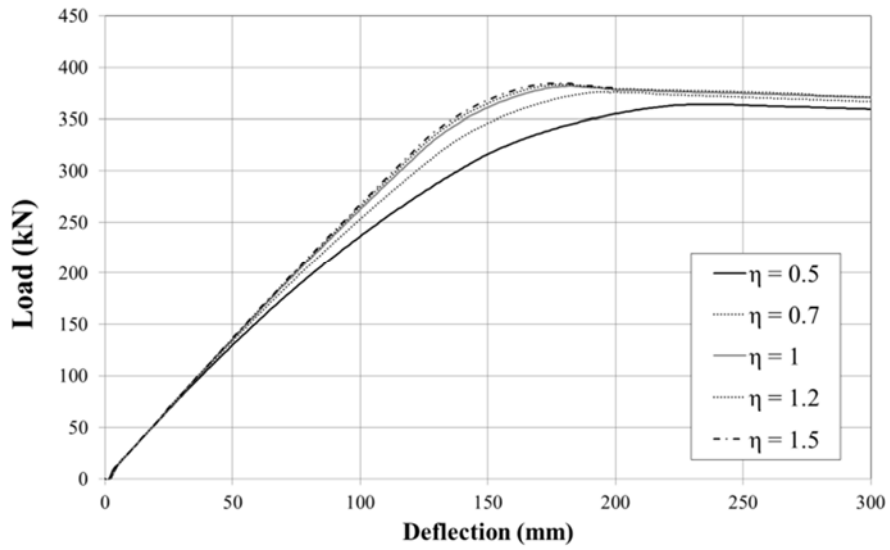


Figure 13: Stress distribution using FE and rigid-plastic analysis (a) beam cross-section, (b) $\eta = 1$ and (c) $\eta = 1.7$.

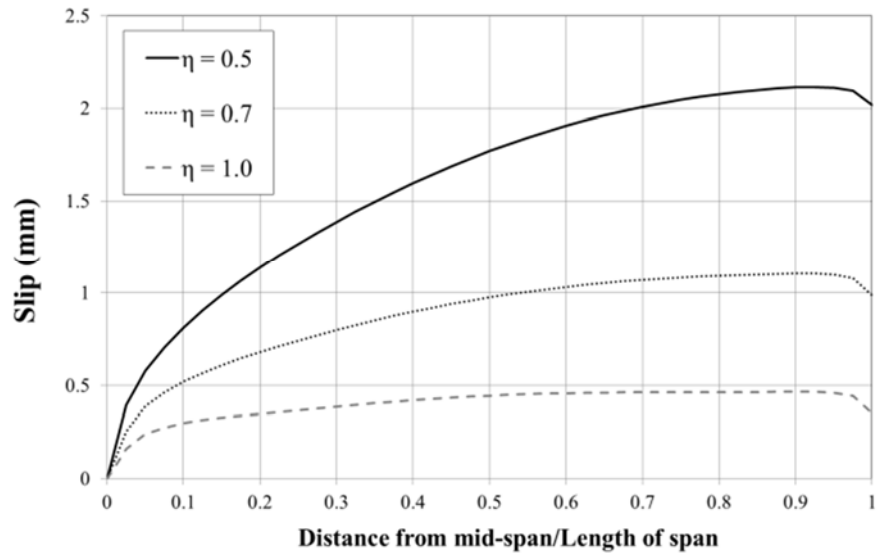


(a)

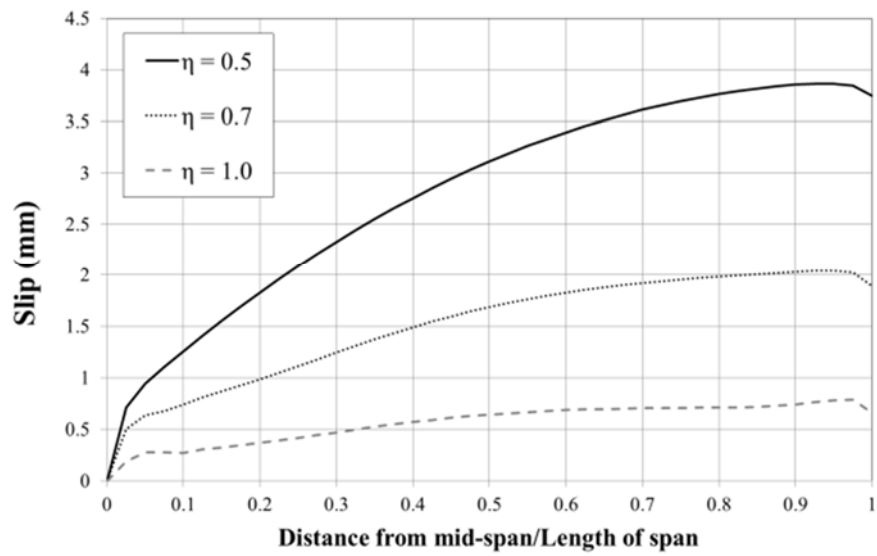


(b)

Figure 14: Effect of shear connection ratio on the flexural behaviour of composite beam for composite beams made from (a) S460 and (b) S690

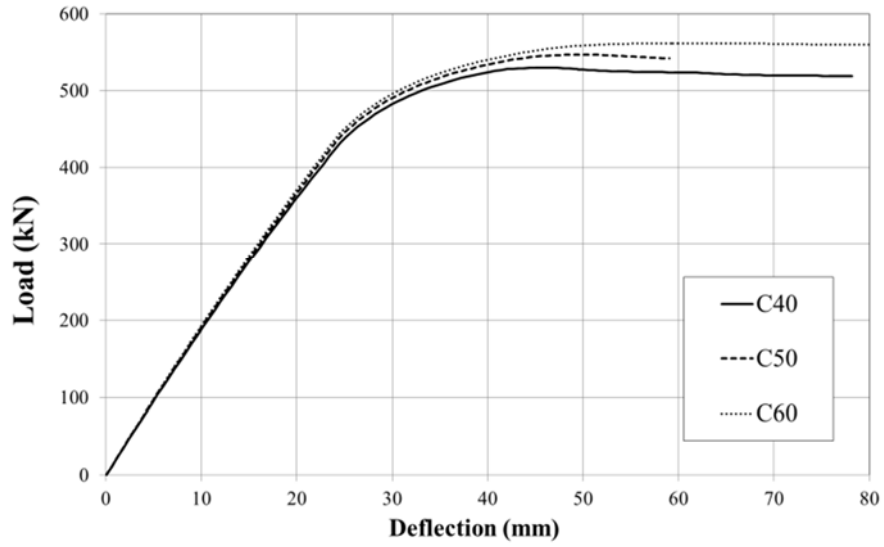


(a)

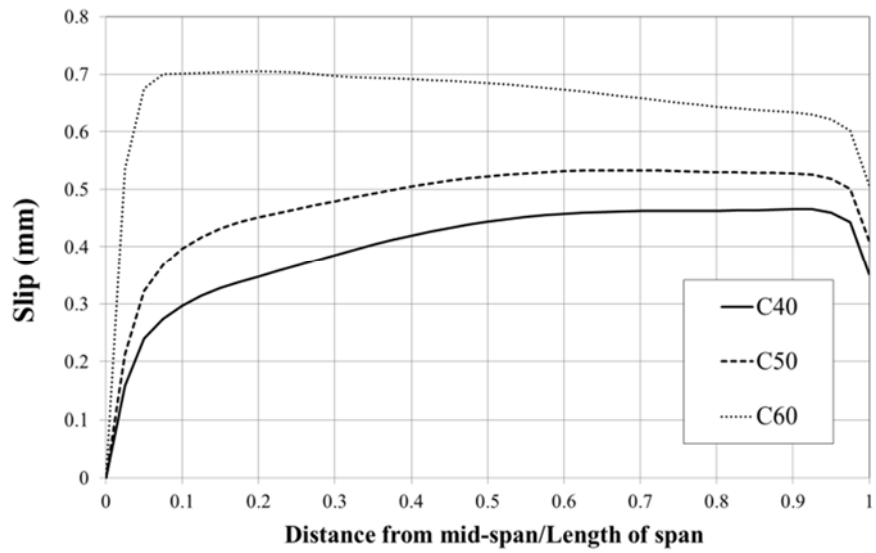


(b)

Figure 15: Effect of shear connection ratio on the slip distribution of a composite beam made from (a) S460 steel and (b) S690 steel

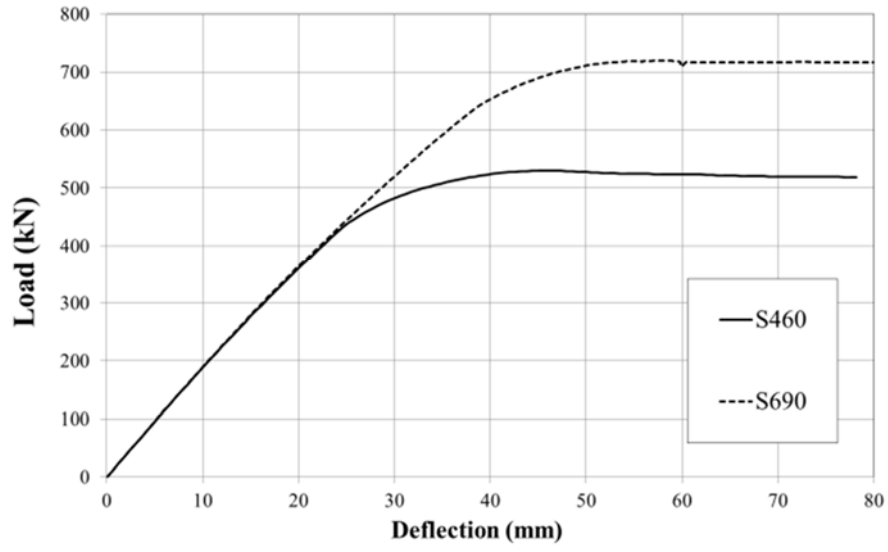


(a)

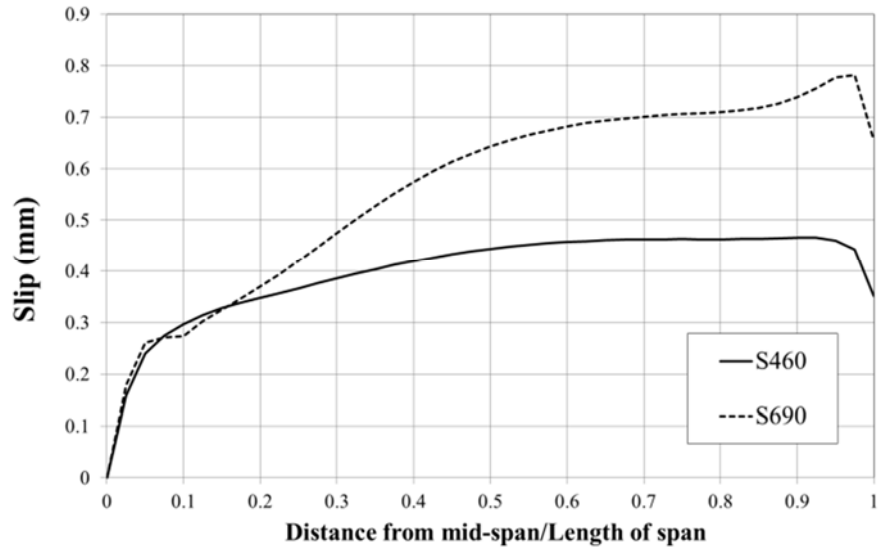


(b)

Figure 16: Effect of concrete strength on the (a) load-deflection relationship and (b) slip distribution of a composite beam made from S460 steel



(a)



(b)

Figure 17: Effect of steel grade on the (a) load-deflection relationship and (b) slip distribution of a composite beam made from C40 concrete

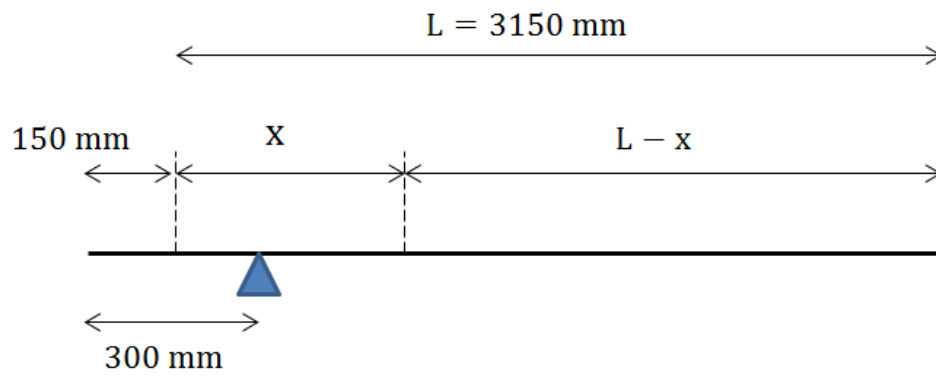


Figure 18: Distribution of shear connectors for analysis of Beam 1

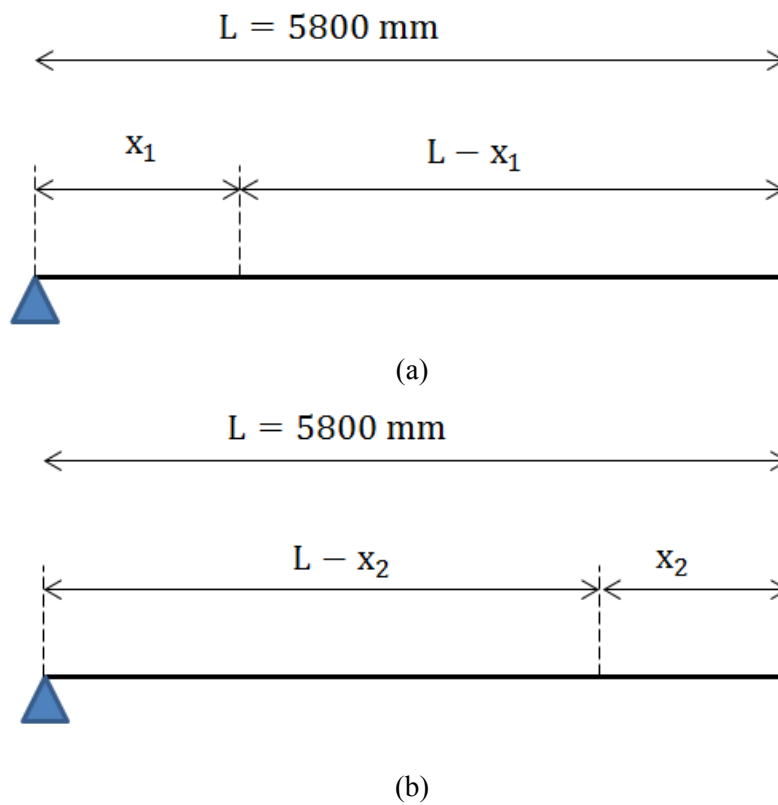
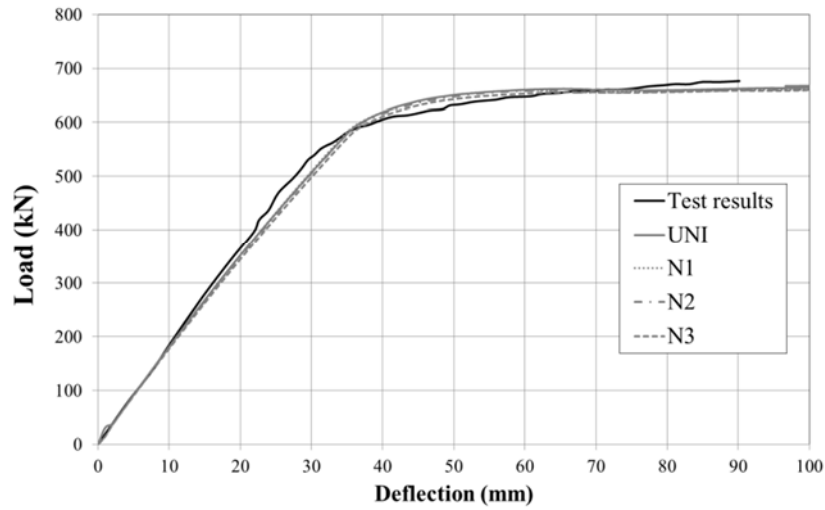
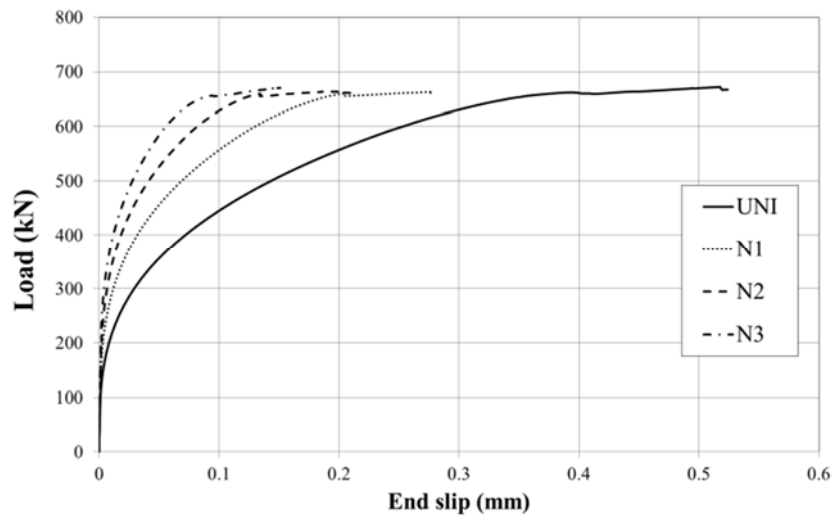


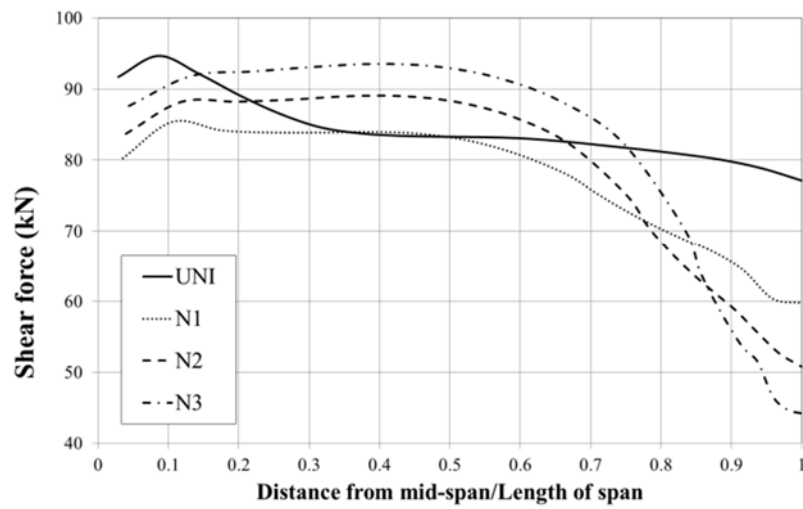
Figure 19: Distribution of the shear connectors for analysis of Beam HASSA-30BS



(a)

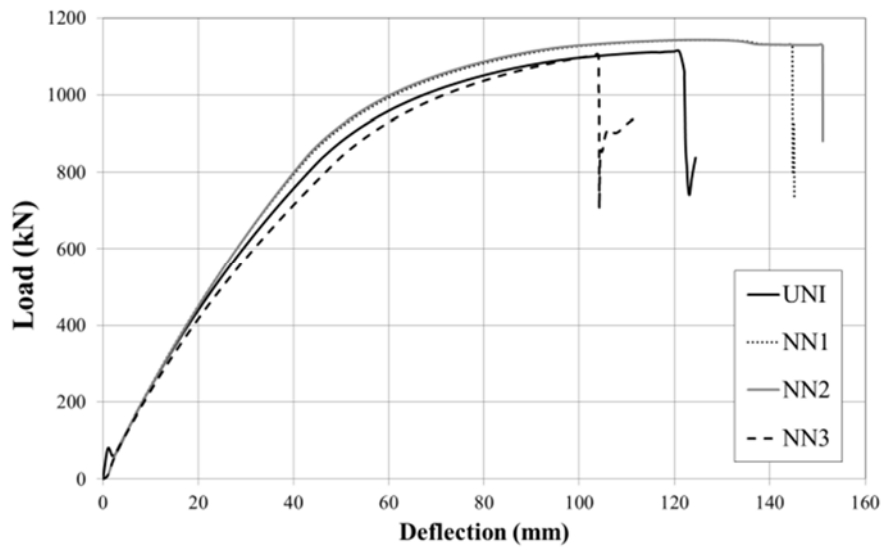


(b)

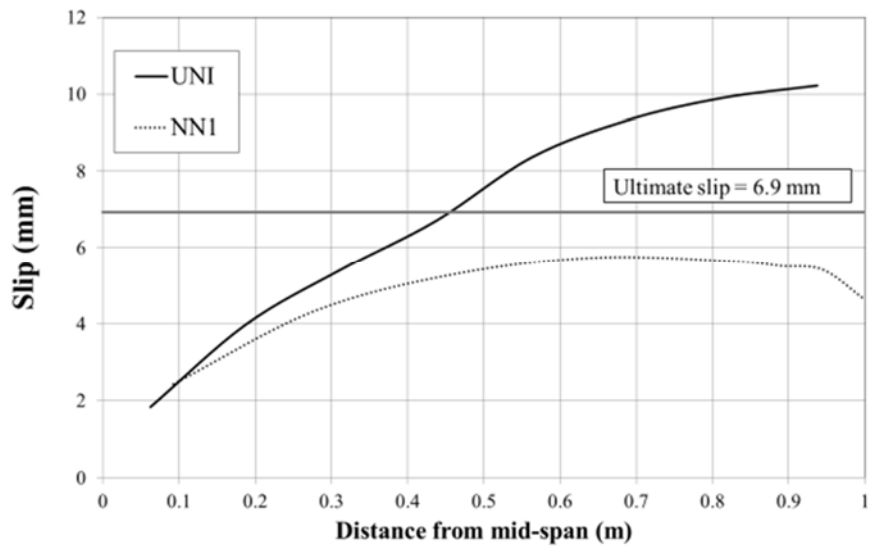


(c)

Figure 20: Analysis of Beam 1 (a) load-deflection curves (b) load-end slip curves and (c) shear forces induced in the shear connectors along the span



(a)



(b)

Figure 21: Effect of shear connector arrangement for Beam HASAA-30BS (a) Load-deflection response and (b) slip induced in the shear connectors along span

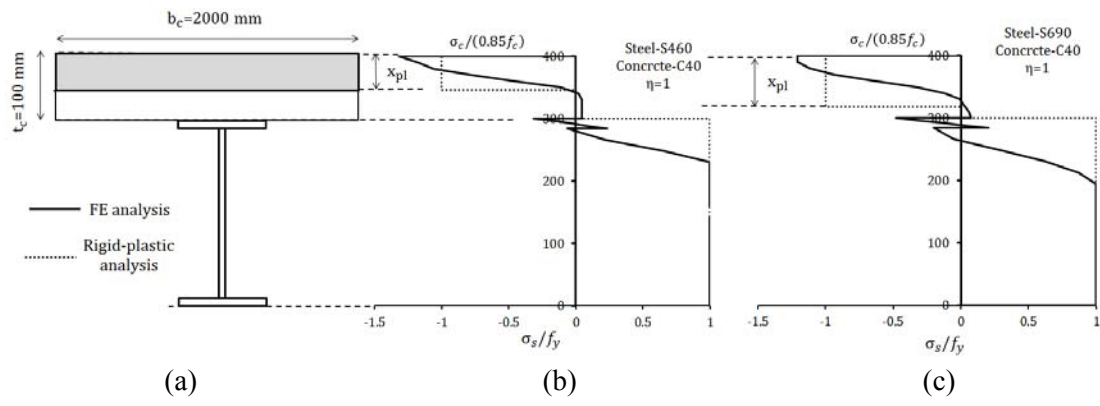
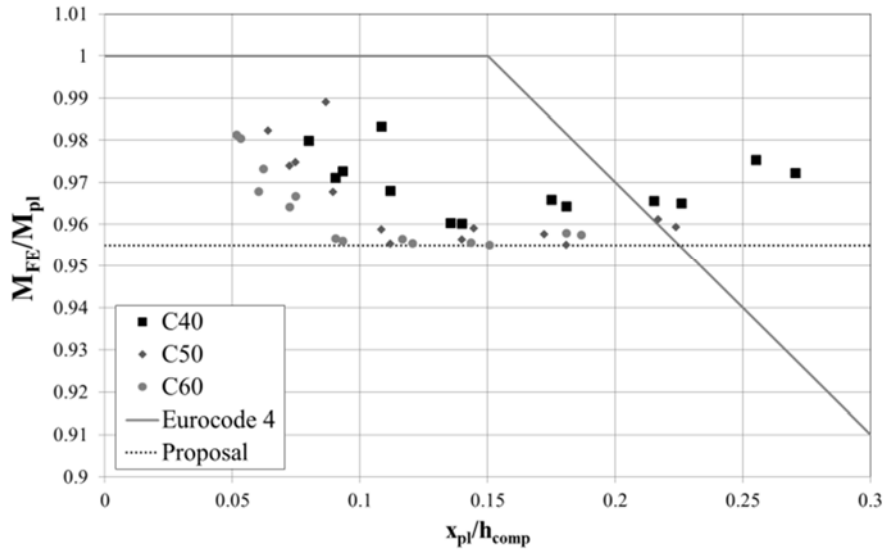
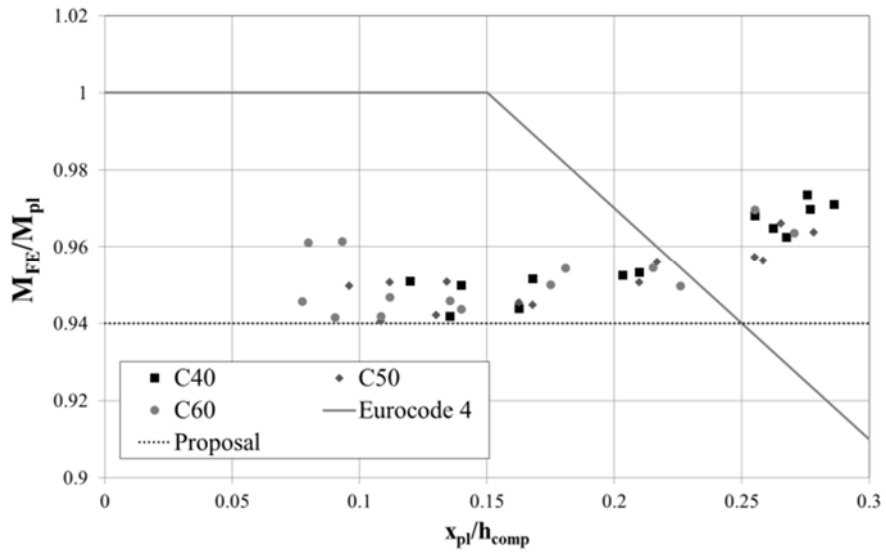


Figure 22: Stress distributions using FE and rigid-plastic analysis (a) beam cross-section (b) S460 steel and (c) S690 steel

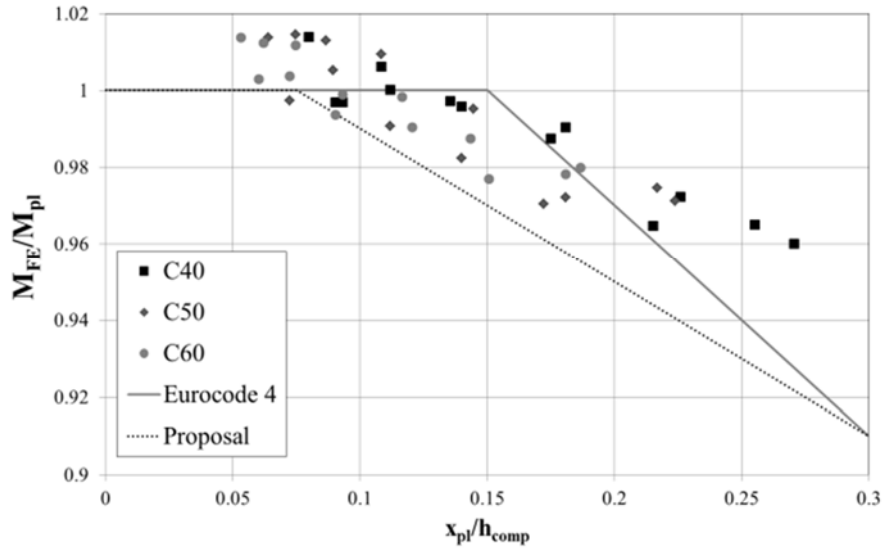


(a)

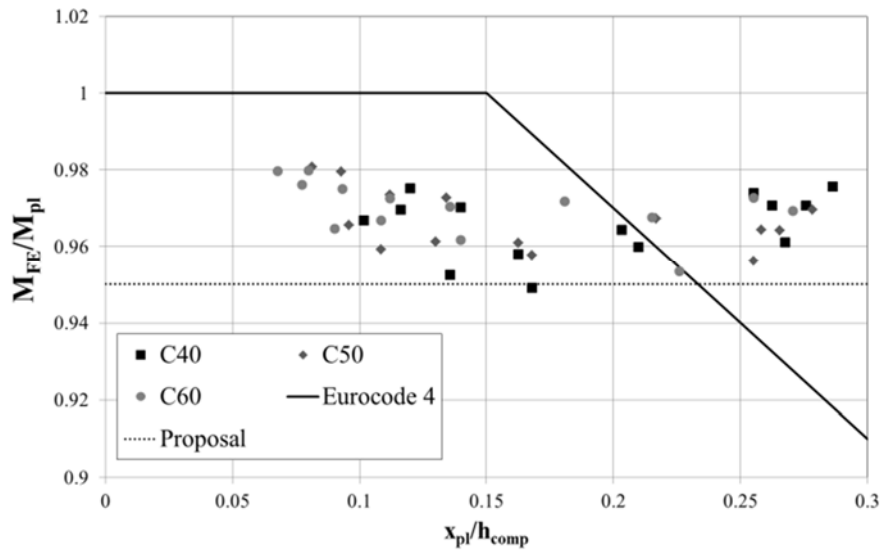


(b)

Figure 23: Reduction factors for composite beams made from (a) S460 HSS and (b) S690 HSS



(a)



(b)

Figure 24: Reduction factors for composite beams made from (a) S460 HSS and (b) S690 HSS

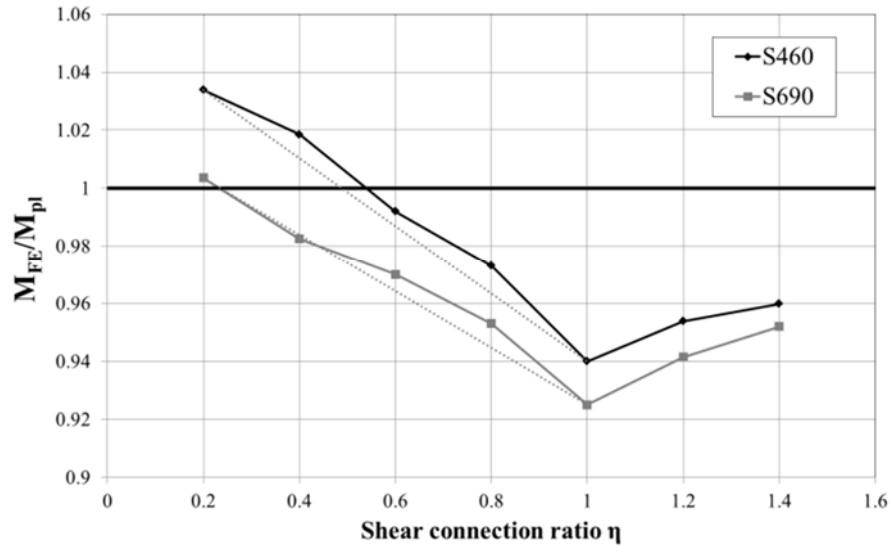


Figure 25: The effect of the degree of shear connection on the flexural capacity of the composite beam with profiled sheeting